



# Production of CNC from agro-waste biomass (maize shells) as a potential reinforcement in bio-nanocomposites: Extraction, modification, and characterization study

M Mohinur Rahman Rabby<sup>b</sup>, Md.Mahmudur Rahman<sup>a,\*</sup>, Bijoy Chandra Ghos<sup>a</sup>, Md.Abdul Gafur<sup>c</sup>, Md. Al-Amin<sup>a</sup>, Shamim Dewan<sup>b</sup>, Md.Ashraful Alam<sup>d</sup>, Md.Ismail Hossain<sup>a</sup>

<sup>a</sup> BCSIR, Rajshahi Laboratory, Bangladesh Council of Scientific and Industrial Research (BCSIR), Rajshahi 6206, Bangladesh

<sup>b</sup> Department of Chemical Engineering, Rajshahi University of Engineering and Technology (RUET), Rajshahi 6204, Bangladesh

<sup>c</sup> Pilot Plant and Process Development Centre, Bangladesh Council of Scientific and Industrial Research (BCSIR), Dhaka 1205, Bangladesh

<sup>d</sup> Institute of Glass and Ceramic Research and Testing (IGCRT), Bangladesh Council of Scientific and Industrial Research (BCSIR), Dhaka 1205, Bangladesh



## ARTICLE INFO

### Keywords:

Agro-waste biomass  
Green environment  
Cellulosic fibers  
CNC  
Acid hydrolysis  
Ecofriendly biocomposite

## ABSTRACT

Cellulose nano crystal (CNC) has been considered as multifunctional biopolysaccharide due to its outstanding properties and biodegradable nature. CNC was derived from agro-waste namely maize shells by different treatment like soaping, alkali treatment, bleaching, and acid hydrolysis. Maize shells were chosen as it is considered a waste material that has no use rather burning. While burning of these releases exposes a considerable amount of environmentally airborne pollutants which are responsible for global warming. However, the properties of the extracted CNC were characterized by using FTIR-ATR, XRD,TGA,DTA,DTG, FESEM, DLS, UV-vis-NIR, and Zeta-potential analysis. The removal of hemicellulose and lignin were expelled from CNC asserted by FTIR-ATR. FESEM was used to capture microstructure and surface morphology. TGA/DTA/DTG was used for measurement of thermal stability. Phase composition, crystal structure/exact atomic position were analyzed by XRD measurement. The CNC was found more thermal stability (exposing 40 % residual mass at 600 °C), high crystallinity index ( $76.09 \pm 0.91\%$ ) with good structural purity and smaller particle size around 100 nm along with negative zeta potential. Due to these outstanding properties the newly produced CNC could be beneficially used as a potential reinforcement in bionanocomposite fabrication for various uses in biomedical, industrial, and engineering sectors for the development of sustainable environment.

## 1. Introduction

A Green environment is a major concern across the globe. Specifically, Bangladesh has anxiety (as a developing country) about its environment to protect against the non-biodegradable materials (Rahman et al., 2023b; Ng et al., 2015a, 2015b; Rahman et al., 2024c). With growing industrialization, the use of polymers has increased due to their potential physicochemical properties (high persistence) and economic compatibility. The development of easily usable commodities, which are preliminary extracted from petroleum, results in synthetic polymers being dumped into municipalities, termed as solid waste (Hossain et al., 2024; Kumar et al., 2022; Song et al., 2009; Rahman et al., 2024e; Kabir et al., 2018). These non-biodegradable synthetic polymers are complex to reuse, and incineration of these polymers leads

to the release of toxic pollutants, including polychlorinated biphenyls (PCBs), furans, and dioxins, which impose lethal impacts on the ecosystem (Kabir et al., 2020). Their contact with the environment contaminates the ecological system by incorporating into the food chain, depending on plastic density, i.e., PP ( $0.85\text{--}0.95\text{ g cm}^{-3}$ ), PA ( $1.38\text{--}1.45\text{ g cm}^{-3}$ ), PVC ( $1.1\text{--}1.58\text{ g cm}^{-3}$ ), PE ( $0.90\text{--}0.99\text{ g cm}^{-3}$ ), PEST ( $0.95\text{--}1.1\text{ g cm}^{-3}$ ) which can convey carcinogenic diseases, i.e., cancer, obesity, and infertility (Kumar et al., 2022). Monomeric building blocks and additives of plastics, i.e., Di (2-ethylhexyl) phthalate (DEHP), polybrominated diphenyl ethers (PBDE) and BPA (Bisphenol A) compounds, stimulate human health hazards and have a deleterious impact on health when exposed to certain concentrations (Halden, 2010; Rodrigues et al., 2019). BPA has a potent deleterious impact on generation and health, i.e., aggressive behavior, decreased male fertility, early sexual

\* Corresponding author.

E-mail address: [shamrat.acce@gmail.com](mailto:shamrat.acce@gmail.com) (Md.Mahmudur Rahman).

maturity, and so on. Consequently, the uses of BPA in infants' bottles and spill-proof cups has ceased in the USA. Likewise, DEHP has detrimental health impacts such as increased waist circumference, changes to the female and male reproductive systems, and insulin resistance (North & Halden, 2013). To mitigate the lethal impacts on human health and the environment, there must be an increased concern regarding the use of biopolymers that can be derived from natural plant or animal sources, i.e., cellulose (Rahman et al., 2024f; Hassan et al., 2024, 2024a) and chitosan (e.g., Shrimp shell) respectively (Rahman & Maniruzzaman, 2023; Kabir et al., 2020; Rahman et al., 2024 g). Cellulose is a primary plant, secondary plant, and animal-originated biopolysaccharide that is inclusively attainable in nature (Rahman et al., 2023c; Seddiqi et al., 2021, 2024b). The classification of cellulose is disclosed in Fig. 1 based on its origin Blanco et al. (2018); Ng et al. (2015b); Rahman et al. (2023c); Seddiqi et al. (2021). Although cellulose is abundant in woody plants, the continuous use of these has led to deforestation. To remedy this situation, scientists are searching for suitable nonwoody sources, which can be classified into two groups: primary and secondary plants, for their dynamic induction. Primary plants are produced for the mere use of fiber, while secondary plants cultivate diverse objects that produce byproducts, such as maize shells, banana rachis, okra bast, sisal leaf, corn cob, and so on (Rahman et al., 2018a & 2023b; El Messaoudi et al., 2024). Furthermore, agro-waste from secondary plants is sometimes larger than their edible parts, e.g., *Zea Mays* (cob and shells); these waste parts are not consumed by animals (not used as cattle feed). Therefore, the disposal and burning of this waste led to clogged drainage systems during the rainy season and airborne pollutants, respectively. The utilization of natural source to extract CNC could be prominent for its potential properties, such as antimicrobial, antifungal, large surface area, thermal stability, crystalline properties, biodegradability, biocompatibility, adaptable surface chemistry, nontoxicity, low cost, light weight, low abrasiveness, renewability, high electric resistance, and stiffness, in response to the growing demand for eco-friendliness (biodegradable), and sustainability (Eyley & Thielemans, 2014; Kabir et al., 2020; Liu et al., 2015; Rahman et al., 2023b; Sanjay et al., 2016; Trache et al., 2017). CNC can be employed as a carrier in drug delivery through ionic interaction, which can contribute effectively to the pharmacological field. CNC extracted from maize shell can be applied as a reinforcing agent in composite form to enhance the tensile strength of materials, including automotive coatings and films, biomedical applications (to make biocompatible equipment such as reinforcing agents in

hip implants), and electronic parts that reveal considerable desired tensile strength. It can impart suitable drug loading through pharmaceutical nano formation due to its enormous microstructure and surface charge, which shows convenient dispersion in a colloidal medium. CNC has some important properties, i.e., ionic medium (which enhances immobilization), inertness, physical stability, reduction of product inhibition, and enhancement of enzyme activity, which makes it appropriate as a support matrix (carrier matrix) that can be used in drug delivery to immobilize enzymes. An inert and highly stable support matrix confines the enzyme within a suspension by forming van der Waals forces, hydrogen bonding, or hydrophobic interactions (Datta et al., 2012). The extracted CNC from maize shell reveals upright properties; thus, it could perform as an enzyme activator (Maheri et al., 2022). In vivo studies arises awareness of the application of CNC in the human body (through drag delivery) regarding the fate and toxicity of nanocellulose, which may pose issues of health effects upon skin contact or injection (Kalhorri et al., 2022; Seabra et al., 2018). Nowadays, renewable and sustainable biobased materials are a key consideration. The enormous characterization property of the extracted CNCs could be beneficially used in the future in the fields of biomedical (making body armor by developing the crystal structure of CNC in the composite matrix), automotive (reinforced with nanocellulose to develop high-strength, lightweight car body parts that are usually applied in composite form), food industries (alternatives to synthetic additives that work as stabilizers in food products by improving texture), paper, films (improving strength and barrier properties (Vinod et al., 2020), and packaging (developing biofilms (Vinod et al., 2023; Janeni & Adasooriya, 2021)), filters (used in wastewater treatment by forming composites with activated carbon that reveal a larger surface area and greater proficiency in filtration for a longer time (Rahman et al., 2024d)), paints and coatings (reinforcing color retention properties, high thermal resistance, scratch resistance, abrasion resistance, and UV resistance without any changes in visual observation), adhesives (increasing shear forces), cements (reinforcing composites by increasing the strength of cement and the formation of calcium-silicate-hydrate gel), plastics (used as additives that enhance the thermal and elastic properties of plastics due to the good dispersion of CNC in a polymeric matrix (Hossain et al., 2024)), and electronic and energy storage (developing extensive thermal and strength properties of supercapacitors and other electronic parts that are sensitive to heat and breakage) (Ng et al., 2015a). The scientists worldwide have insisted on

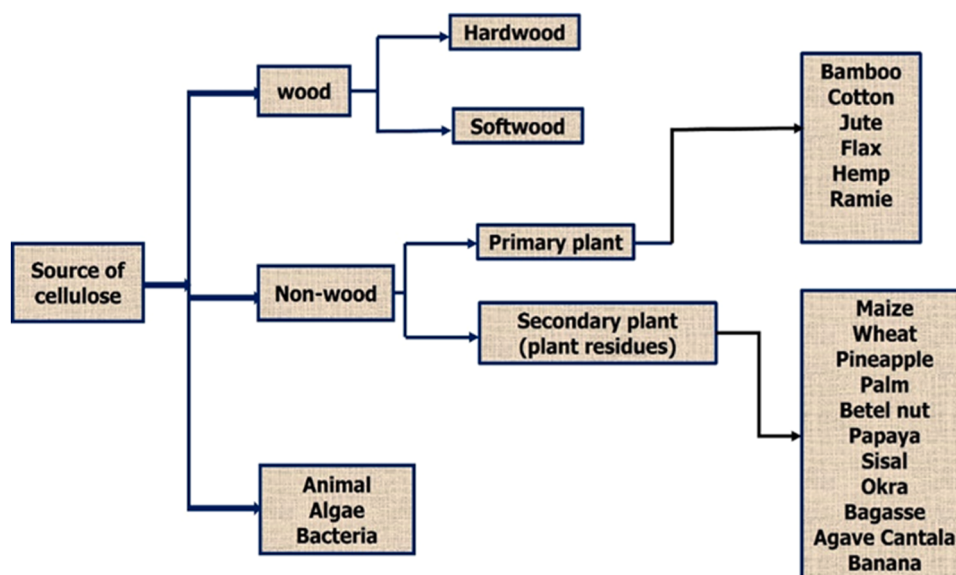


**Fig. 1.** Distribution of cellulose based on (a) woody, (b) non-woody, and (c) animal or microbial related diversity as various sources (primary, secondary plant and microbials).

their interest in CNC to find the more economical and potential sources by focusing on secondary plants (non-wood) to reduce the pressure on woody plants, which could be instrumental in eliminating deforestation. A plenty of natural sources exist that produce unusable byproducts that are rich in cellulose content and are suitable for producing highly pure CNC. A few, such as sugarcane, maize, keya, and banana, are the key sources of cellulose that generate wastes like sugarcane leaf sheath, maize cob, maize shell, keya leaf, banana rachis, asparagus bean stem fiber, Ficus macrocarpa bark, etc., (Hassan et al., 2024; Hossain et al., 2024; Rahman et al., 2024a & 2024e; Tengsuthiwat et al., 2024a & 2024b). Cellulose is the structural organic polysaccharide composed of link by a linear  $\beta(1,4)$ -glycosidic bond where the monomer unit is named d-glucose. The functional group, i.e. -OH, is responsible for the setup by  $\beta$ -conformation along the plane of the anhydro glucose unit (Coseri, 2017; Lu & Hsieh, 2010). Cellulose is constructed a with number of repeating units (monomer) termed glucose that contains divers -OH groups ( $-3$  OH groups), which steer the physical properties and crystalline array of cellulose by forming hydrogen bonds (intra- and inter-molecular). This property makes the structure identical as a basis for photonic and adaptive materials, i.e., easily adapting color and shape (Almeida et al., 2018; Blanco et al., 2018; Pérez & Samain, 2010). The present -OH groups can expose reactive faces and bind functional groups when numerous treatment methods are applied (mechanical, chemical) to form crystalline nanocellulose (Blanco et al., 2018; Mondal, 2017; Pérez & Samain, 2010; Rahman et al., 2023d). Cellulose reveals polarity when molecular dissimilation emerges due to electronegativity; modifications could arise due to sensitivity to the consolidation of the end chain. Thus present ring oxygen atom and hydroxyl group reveal reactions, i.e., deoxygenation, acylation, etherification, and oxidation reactions. Deoxygenation means the removal of molecular oxygen from cellulose; it is crucial due to its hydrophilic property, which is not advantageous for the crystallinity of cellulose and can be accomplished by substituting hydroxyl group with others, i.e., amino group (Pérez & Samain, 2010). The invention of natural fiber sources for cellulose extraction is a major prospect worldwide to enhance the unique or more adoptable materials properties. Cellulose is enormously available in woody plants; nevertheless, their use has been diminished due to lower cellulose content and the complexity of structure (hardwood) in removing components (hemicellulose, lignin and others) through mentionable treatments (Siró & Plackett, 2010; Stelte & Sanadi, 2009). Elsewhere, nonwoody plants generate by-products (waste) that are used as alternative sources of cellulose (Marques et al., 2010) due to concise growth time and easy to extraction; however, there are numerous limitations, such as high silica content and economic viability for generation in developing countries (Blanco et al., 2018; Kalia et al., 2014). The challenge is sorting out the absolute source of cellulose, so a plethora of nonwoody source of cellulose has been tabulated in Table 1 and assimilated with this study (Maize shell). Maize (*Zea Mays*) is the third

most produced grain in Bangladesh and the second most in the world which is cultivated twice a year in Bangladesh. Byproducts (shell and cob) are the mentionable source of cellulose where the shells of maize are rich in natural fiber (Erenstein et al., 2022). Millions of tons (about 1.8) of maize are consumed per year in Bangladesh, and the increasing cultivated land and demand for production of maize would be doubled by 2050 (Adnan et al., 2021). Globally, 137 million tons of dry maize are cultivated on approximately 197 Million hectares of land (Erenstein et al., 2022). A CNC extraction and characterization study has been conducted to eliminate the evolved drawbacks by using this potential waste source. Although several studies have been conducted to develop nanocomposite properties through various chemical and mechanical treatments, nevertheless, the presence of -OH groups in the cell wall, which form hydrogen bonds in the molecular structure of cellulose, exposes cellulose to its hydrophilic nature (having an affinity for water and alcohol). This property could impose a negative impact on composite materials. This study will focus on mitigating this drawback by hindering this reaction with congenial controlled methods. A portion of the work has been done to extract CNC from the waste of maize, but no one has performed extractions of CNC from the shells of a particular variety of maize, namely *Zea Mays*. The shell of *Zea Mays* has no economic value and isn't used as cattle food. Consequently, this feature would be sound for extracting CNC from the shell by utilizing this unique abundant source of cellulose, which could assist in numerous fields of application as a potential reinforcement in bio-nanocomposites. The production of CNC from this particular variety of maize shell is still unbeaten. Hence, this study will cover the following prospects to address complexity in bio-nanocomposites by accelerating their reinforcement properties: (a) to provide a report developing a new route for the production of CNC, (b) to optimization the physiochemical, thermo-mechanical, and morphological properties of the extracted CNC, and (c) to inaugurate notable new applications. (Fig. 2 and Fig. 3)

## 2. Experimental

### 2.1. Materials

*Zea Mays* shells were collected from the local area of the BCSIR Rajshahi laboratory campus. GHARI detergent powder was purchased from the local market, manufactured by RSPL Health BD LTD (Bangladesh). Sodium hydroxide (NaOH; purity  $\geq 97\%$ ), sulfuric acid ( $H_2SO_4$ ; purity of about 98 %) were purchased from Merck Specialities Private Limited (INDIA). Sodium metabisulphite ( $Na_2S_2O_5$ ; purity 97 %), Sodium Chlorite ( $NaClO_2$ ; purity min. 80 %) were purchased from RESEARCH-LAB FINE CHEM INDUSTRIES (INDIA). HCl (purity about 37 %) was purchased from Merck Life Science Private Limited (INDIA), ethanol ( $C_2H_6O$ ; Purity 96 %) was purchased from Supelco Merck (Germany). DI (Deionized) water was collected from BCSIR Rajshahi

**Table 1**

The lignocellulosic contents and chemical composition of different types of natural fiber (based on source) are abundant in Bangladesh.

Fiber name	Cellulose %	Hemi-cellulose %	Lignin %	Density (g/cm <sup>3</sup> )	Moisture %	References
Mesta	48	14	36	1.46	13	(Rahman et al., 2023b)
Sisal	67–78	10–14.2	8–12	1.450	11	(Mishra et al., 2004; Sreekumar et al., 2009)
Hemp	76.12	5.65	12.28	0.86	7	(Baltazar-y-Jimenez & Bismarck, 2007; Kostic et al., 2008; N. Lu & Oza, 2013)
Sugarcane leaf sheath	54.40	21.75	11.52	1.2–1.5	8.74	(Hassan et al., 2024)
Keya leaf	54.37	21.57	12.15	1.2–1.3	7.41	(Hossain et al., 2024)
banana (M. oronta) tree rachis fiber	63.10	11.01	8.63	1.2–1.5	9.17	(Rahman et al., 2024e)
Maize cob	52	28	15	0.82	–	(Dewan et al., 2024)
Jute	60–61	13	8–13	1.5	12.5	(Rahman et al., 2023b)
Flax	75.2	8.6	4.8	1.28–1.3	7	(Amiri et al., 2017; Baltazar-y-Jimenez & Bismarck, 2007)
Bamboo	73.8	12.5	10.1	0.66	–	(Li et al., 2002; Naim et al., 2022)
Agave cantala	68–70	15–17	6–7	1.45	10–12	(Rahman et al., 2023b)
<b>Maize shell</b>	<b>58–60</b>	<b>20–25</b>	<b>14–16</b>	<b>0.8</b>	<b>8–10</b>	<b>This study</b>

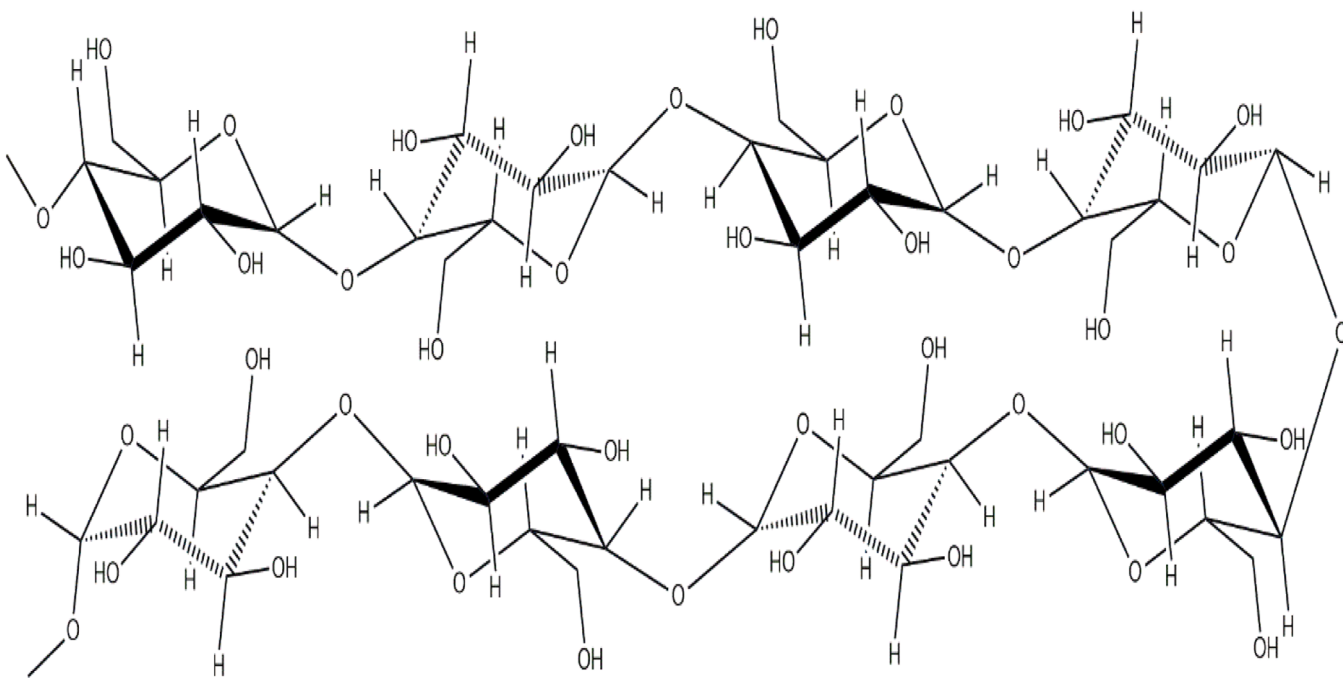


**Fig. 2.** Molecular network structure of the  $\alpha$ -cellulose that belongs to the naturally available plant fibers.

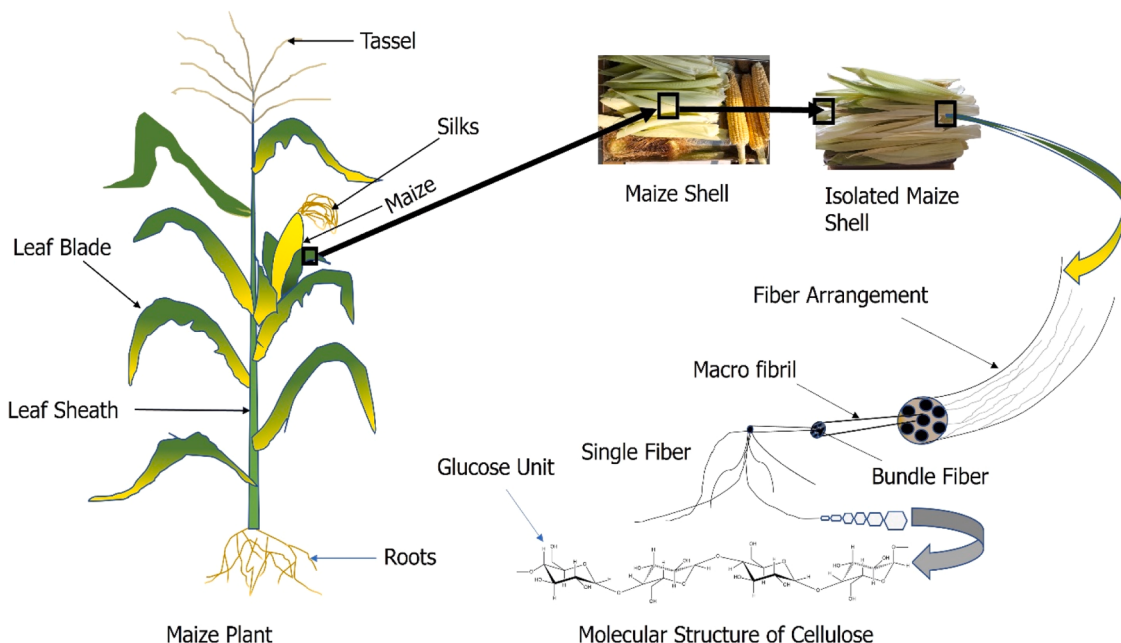


**Fig. 3.** Schematic description/Overall route map of molecular cellulose from secondary plant (particularly maize plant).

Laboratory.

## 2.2. Methods

### 2.2.1. Extraction of maize (*Zea Mays*) shell fiber

A specific variant of maize (*Zea Mays*) had been collected from the BCSIR Rajshahi Laboratory Area. The edible and inedible parts were naked from maize, which exposed types of inedible parts, i.e., cob, shell, and silks. The shells were separated to obtain dried raw fiber from its hard form. The raw fiber can be extracted via several types of techniques, i.e., Dew Retting, Wet Retting, and Mechanical Extraction, respectively (Rahman et al., 2023c). The extraction process was

performed through mechanical hammer milling due to its more prominent characteristics, i.e., fast, easy, cheap, and small in size. Prior to milling, the shell's size was reduced as much as possible for proper milling. After milling, the extracted raw fiber was placed in an electric vacuum oven manufactured by BINDER GmbH (Germany) and dried in the oven at 105 °C for 2 hours. After drying, the dried raw fiber was collected for further use. The overall process has been depicted in Fig. 4 and Fig. 5.

### 2.2.2. Soaping of maize shell

The exclusion of dust, dirt, oil, waxy, and gummy substances from maize shells by using a soap solution is called scouring. The dried raw

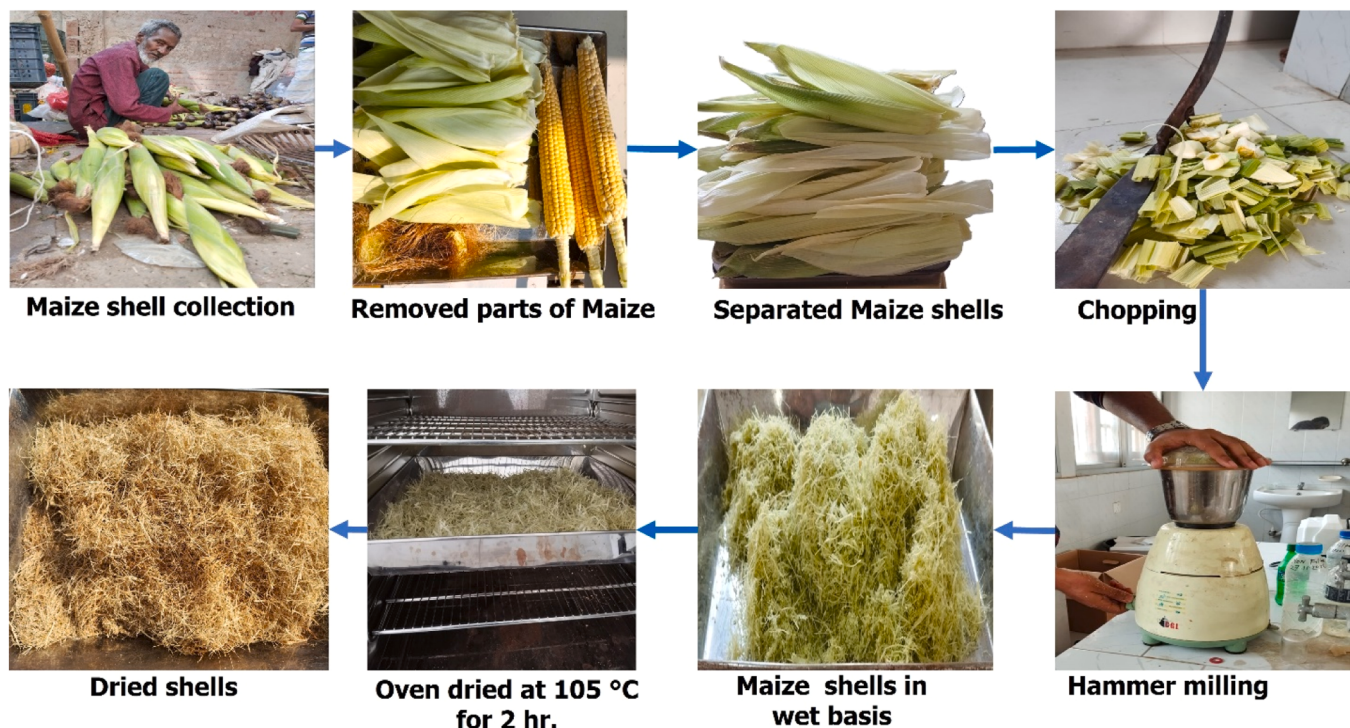


Fig. 4. Collection and isolation of raw fiber from maize shell by applying several mechanical operations.

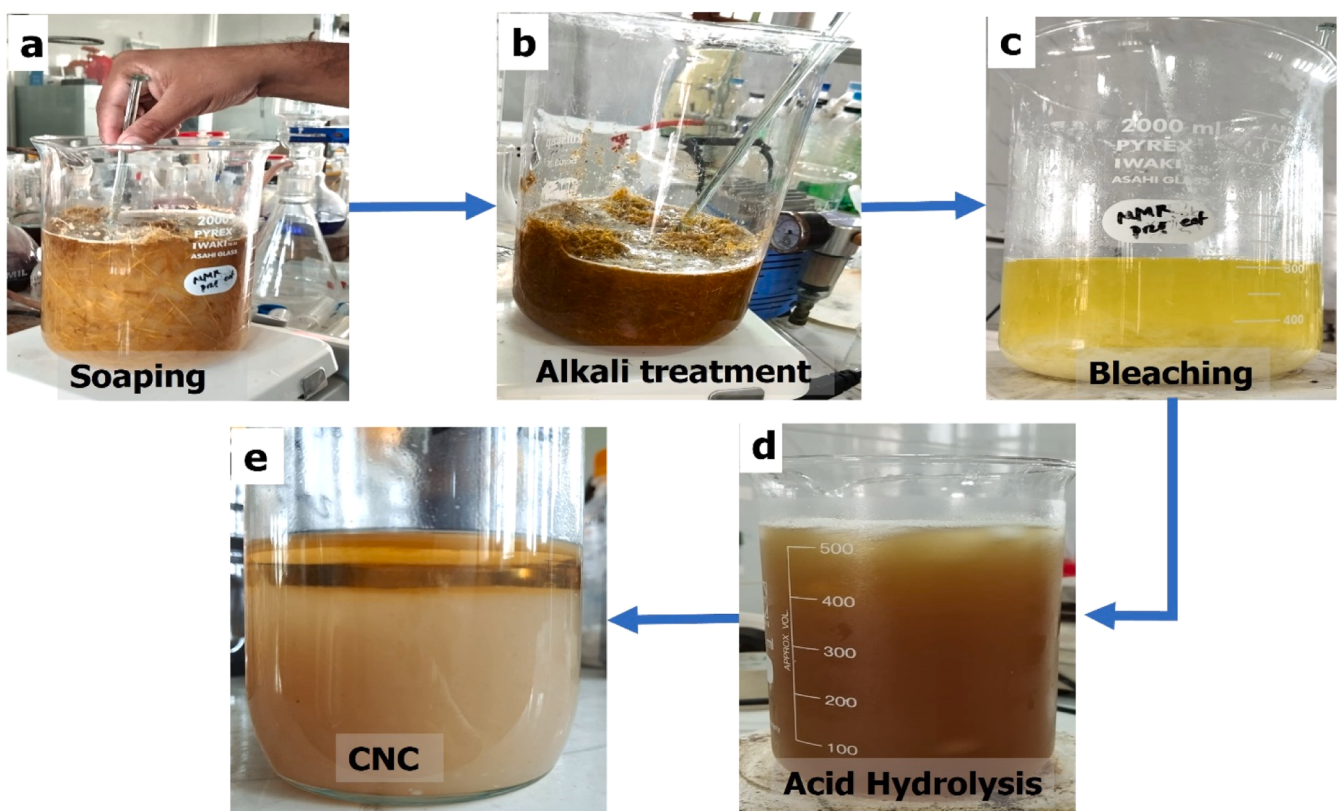


Fig. 5. Schematic diagram and isolation of CNC from raw fiber through several chemical treatment operations.

fiber was scoured via moderate stirring in a 1:15 ratio with a 2 % soap solution at room temperature for 1.05 hr. The soap solution was prepared from GHARI detergent powder diluted in distilled water, which acts as a surface-reacting agent (Rahman et al., 2018b; Rahman &

Maniruzzaman, 2021; Rahman et al., 2024b). The scoured fiber was washed properly with distilled water and placed in an electric vacuum oven at 105 °C for 2 hr. After that, the dried shell was preserved for alkali treatment.

### 2.2.3. Alkali treatment

The raw fiber encompasses cellulose, hemicellulose, lignin, and other mineral content. These entities have several properties and impacts on industrial applications. Currently, a major concern is to protect nature through the enormous use of biodegradable composites. Henceforward, CNC is the most prominent multifunctional biodegradable compound which is produced from bulk cellulose. That's why other components (except cellulose) from fiber need to be eliminated through different chemical treatments. As a part of this, the hemicellulose content has been eliminated from the scoured shell by alkali treatment. The treatment was conducted through a 16 % NaOH solution in a 1:15 vol ratio via moderate stirring on a hot plate at 50 °C for 1 h (Rahman et al., 2023b). Subsequently, the treated shells were washed with distilled water by placing them on filter cloth to diminish the loss, and the residue was dried in an electric vacuum oven at 105 °C for 2 h. Then the alkali-treated shell was preserved for the bleaching operation.

### 2.2.4. Bleaching

Bleaching is the process widely used to conduct remove lignin content from fiber. The technique involves immersing the fiber in a mixture of two or more individual chemical solutions, and during the treatment, a basic or acid solution is needed to maintain the pH level at 4. Maintaining the pH level is necessary to eliminate the risk of injury to its functional properties or losses in cellulose content from the fiber. Consequently, a 2 % sodium chlorite ( $\text{NaClO}_2$ ), and a 2 % sodium metabisulphite ( $\text{Na}_2\text{S}_2\text{O}_5$ ) solution were used for the treatment, and 0.1 N HCl or 0.1 N NaOH was used to maintain the pH at 4 (Rahman et al., 2023c; Hassan et al., 2024). Initially, the alkali-treated (dried) raw fiber was immersed in the 2 %  $\text{NaClO}_2$  solution in a 1:20 vol ratio and treated at 90 to 95 °C for 2 hr with moderate stirring on an electric hot plate. During the process, 0.1 N HCl was successively added after a time-lapse, and the solution pH was checked using a pH meter. The  $\text{NaClO}_2$ -treated solution turned yellowish, then the fiber was rinsed several times with distilled water and appeared mostly white. The rinsed fiber was immersed in a 2 %  $\text{Na}_2\text{S}_2\text{O}_5$  solution at room temperature for 15 min. Subsequently, it was rinsed properly with distilled water by placing it on a filter cloth, resulting in pure white, lignin-free cellulose. The bleached fiber was then in an electric vacuum oven at 105 °C for 2 hr and preserved for acid hydrolysis.

### 2.2.5. Acid hydrolysis

Nano-sized cellulose is the most effective form of biodegradable compound. It has multifunctional properties, by which it secured positions as a dominant agent in industrial and other applications due to its prosperity in nano form. To make particles in nano size, acid hydrolysis is the most prominent method. The technique was conducted by immersing bleached fiber into a 60 %  $\text{H}_2\text{SO}_4$  solution (Rahman et al., 2022; Hossain et al., 2024). Beforehand, the dried bleached fiber was crushed homogeneously into a small size as much as possible. It was then immersed in the acid solution at a 1:15 ratio at room temperature via continuous stirring with a magnet on a hot plate and waited for it to fully dissolve or break down all fiber, which turns into nano form. When the brown color appeared, two-fold ice was poured into the solution to quench the reaction, which tentatively stopped the reaction; otherwise, acid could burn the fiber particles. This acid hydrolysis stage is the most challenging because if the reaction is not quenched at the right time, the quality of CNC will not fall in the outstanding category. If the quenching is done prior to the nano formation, the CNC will not reach the nano level, but if it is delayed in quenching, the cellulose may burn and be destroyed, leaving only a carbon dot or a mixture of carbon dots and CNC. Hence, the hydrolysis reaction time and neutralization are the most challenging segments in acidic treatment, where cellulosic fiber comes into nano form under a controlled reaction of a fixed concentration around 60 % of  $\text{H}_2\text{SO}_4$  solution, which makes this stage most difficult due to the sensitive nature of cellulosic fiber when subjected to acidic medium for a long time (blackish color formed by burning of the

subjected fiber). The stirring was continued until the ice fully melted and diluted the acid with the distilled water ice in a portion that could reduce the acid concentration and terminate the reaction ability. The overall time took about 30 min to complete the process (Sheikh et al., 2023; Rahman et al., 2024d). Consequently, the crystalline nanocellulose (CNC) was collected through the centrifuge and immersed in alcohol (ethanol) for further study.

## 2.3. Characterization methods

### 2.3.1. Fourier transform infrared spectroscopy-attenuated total reflectance (FTIR-ATR) analysis

Fourier Transform Infrared (FTIR) spectroscopy has been deemed a reversible (while after investigation, the sample properties remain intact) scheme that accomplished ascertaining the presence of chemical structure, functional groups, molecular performance (inter/intra molecular collaboration), chemical composition and so on (Rahman, 2024). FTIR-ATR spectra subjected to the raw, alkali treated, bleached, and CNC of polymeric specimen's ranges between 400 and 4000  $\text{cm}^{-1}$  at a specified resolution of frequency, considering several obverse aspects for a sole/individual pattern owing to thorough examination (Rahman et al., 2023c). The equipment used to conduct this specific experiment was PerkinElmer, S.N.- 115,061, Model: L1600300, made in Llantrisant, UK, which was arrayed with a DTGS detector and connected to PerkinElmer Spectrum IR software version 10.6.2, the sample installed directly onto the diamond prism of ATR link-up.

### 2.3.2. Field emission scanning electron microscope (FESEM) analysis

FESEM is essentially performed to distinguish the microstructure and surface morphology of a wide range of specimens by constructing a high-resolution image set down at a nanometer scale with high intensification (Koivuluoto et al., 2010). Subsequently, for superior observation the raw, alkali-treated, bleached fiber, and CNC specimens have been attached to aluminum stubs with carbon tape. Previously, advancements in FESEM analysis of sensitive polymeric materials have been accomplished sputtering via 50 Å gold coating to enhance image quality by reducing the burning effect generated by electron gun (Nallusamy & Manoj Babu, 2016; Williams, 2021). This experiment was performed using a JEOL Model: JSM -IT800, Made in Japan. The position of the specimen and magnification ratio were set precisely to exploit the FESEM micrograph; the micropattern structure has been detected and measured with origin lab software (Deng et al., 2016; Sheikh et al., 2023). Depending on the magnification ratio, the perceptions of pore size can be displayed by focusing on whether it is large or small (Deng et al., 2016). Numerous FESEM images have been taken to obtain more clarity in the characterization test for the perceptible analysis of pore structure.

### 2.3.3. Energy dispersive X-ray (EDX) analysis

EDX analysis is a qualitative and quantitative surface element analysis technique (molecules) and an additional chemical composition documentation technique that provides detailed information (elemental mapping technique) about the subjected polymeric or biopolymers sample. The method was conducted by introducing a specimen to an incident electron beam with 10–20 keV energy supplied, which assaulted the subjected material's surface to release X-rays for the development of an image of molecules present in the specimen (Scimeca et al., 2018). The EDX spectrum exhibits qualitative as well as quantitative information, which is significant for pharmaceuticals, environmental pollution, and other extended analyses by identifying trace elements that are harmful to the ecosystem, along with the morphological behavior of the polymeric sample in the field of application. The FESEM and EDX techniques have been performed using the same equipment (mentioned in FESEM analysis), where the scattered X-ray wavelengths are demonstrated by the semiconductor energy-sensitive detector for the elemental microanalysis of the subjected specimen image. This method

poses some boundaries to extended analysis; i.e., EDS (Energy Dispersive X-ray spectroscopy) can't differentiate between ionic and nonionic elements, which significantly associates with sample assembly under vacuum, the overlap of peak results leading to intermolecular interference, and the difficulty in detecting molecules with less than an atomic number of 5, such as H<sub>2</sub>, Li (Rahman & Maniruzzaman, 2024).

#### 2.3.4. X-ray diffraction (XRD) analysis

XRD is a noninvasive qualitative matrix to clarify the crystalline behavior of any polymeric resources which have a wide applicability to ascertain crystallinity, surface morphology, corrosion assessment, and crystal defects (Bunaci et al., 2015; Whittig & Allardice, 2018). The technique has been carried out to determine the crystallinity index as well as the crystal grain size of polymeric or biopolymeric materials such as raw, alkali-treated, bleached fiber, and CNC specimens. The technique was equipped with an X-ray source, a high voltage generator, and a detector connected with specialized software to display the spectrum and recorded data. The SmartLab SE model X-ray diffractogram of Rigaku company, Japan, was used to explore the samples with a voltage of 50 KV, a current 40 mA, and Cu K $\alpha$  radiation (Rahman et al., 2024c). The sample has been exposed to the 2 $\theta$  angle (fluctuating within the specific ranges) to ascertain the crystalline index, and this parameter was attained by applying the following equation with baseline correction method for better findings:

$$\text{Crystallinity Index, } C_r I = \frac{I_{\text{crystalline area}}}{I_{\text{crystalline area}} + I_{\text{amorphous area}}} \quad (1)$$

Furthermore, Bragg's equation has been applied to ascertain crystal grain size accurately:

$$CS_{000} = \frac{0.89 \lambda}{\beta_{000} \times \cos\theta} \quad (2)$$

Here, Bragg angle positions are denoted by ' $\theta$ ', X-ray wavelength is denoted by ' $\lambda$ ' and ' $\beta$ ' denotes the peak of the full-width at half-maximum.

#### 2.3.5. Thermogravimetric (TGA) analysis

TGA is a conspicuous thermal assessment technique that stands for the measurement of the thermal stability of polymeric or biopolymeric materials against extensive heat employed. TGA commonly provides information about the overall mass transition rate with chemical and physical characteristics by exposure to heat up to 1000 °C (Rahman & Rahman, 2022). The raw fiber, alkali-treated fiber, bleached fiber, and CNC specimen have been engaged at about 25 mg to evaluate individually through EXSTAR 6000 TG/DTA 6300, Seiko equipment. During the inauguration of the experiment, N<sub>2</sub> was used as a purged gas by applying a 50 ml/min flow rate while maintaining a constant heat flow at a specified rate (10 °C/min) that has been assigned by the vendor (Rahman & Maniruzzaman, 2024; Rahman et al., 2024b). The test was performed 2 to 3 times to ensure precise assessment. The differential thermal analysis (DTA) and Derivative Thermogravimetry (DTG) have also been performed using the same device to evaluate other thermal scenarios against specified parameters for the extreme analysis of the specimen. DTA is constructed based on the temperature difference, by which the nature of the reaction is exploited through statistics about reaction kinetics, i.e., endothermic or exothermic. Proper assessment through energy detection can provide materialistic phenomena in different fields of applications, i.e., crystallization, oxidation, sublimation, structural breakdown, and so on (Ravisankar et al., 2014). Through the analysis, materials properties can be enhanced through fabrication with fillers materials that could provide extensive functioning against adverse phases. DTG shows an assessment exactly the same as TGA, which exhibits a thermogram peak against weight and temperature, by which the mass loss rate in mg/min of the subjected polymeric or biopolymeric sample (changes in material weight) can be determined

(Karak, 2012).

#### 2.3.6. Dynamic light scattering (DLS) and Zeta potential (ZP) analysis

The development of a product into a more focused nano form is predominant due to its multifunctional properties. These unique properties and size can be analyzed by the execution of appropriate characterization tests of nanoparticles (Lowry et al., 2016). DLS and ZP are nondestructive commercial characterization techniques used to identify the particle size and determine the surface charge of materials (Bhattacharjee, 2016). These characterization tests can analyze the material's reactivity compared to raw materials. DLS utilizes Brownian motion in colloidal suspension, which is executed by light scattering from dispersed particles over time (Xu, 2008). Zeta potential is a physicochemical constraint that imposes a cognition on the material's size formulation and is performed based on electrostatic force in colloidal suspension to aggregate or stimulate the materials position. The method is disclosed by two parameters, i.e., negative zeta potential and positive zeta potential, which imply the material's affinity in colloidal solution to specify surface charge. Negative zeta potential reveals that the particle present in the dispersion medium is negatively charged. On the other hand, positive zeta potential dictates that the particles in the suspension are positively charged. The magnitude of zeta potential (mV) demonstrates the stability behavior of materials in colloidal suspension because it is affected by the characteristics of the solution medium (Fatfat et al., 2023; Hossain et al., 2024). The particle size analysis technique has been conducted through HORIBA Scientific, Model number: NANO PARTICLE ANALYZER SZ-100V2, Country of origin: Japan which was equipped with a voltage source and connected to a detector. The CNC sample was taken into a cuvette and analyzed by the intensity of light scattering through the suspension, which was displayed in the detector with HORIBA software.

#### 2.3.7. UV-vis-NIR analysis

The CNCs from maize shell fiber were analyzed using UV–Vis-NIR light energy, which is influenced by electronic transitions between molecular orbitals, primarily the HOMO to LUMO transition, of specific functional groups/active binding sites at the molecular level of the subjected biopolysaccharide samples (Hossain et al., 2024). This occurs due to the distinctive way nano-sized cellulose interacts with this particular range of light. The maize shell-derived CNC was examined using this advanced technique to assess its physicochemical properties and structural purity. Additionally, the instrument allowed for the detection of pigments or other color-bearing compounds (Adil et al., 2020). The analysis of CNCs was conducted with a Spectrophotometer (model UV-3600i Plus, Berand: Shimadzu, Country of origin: Japan). The prepared CNCs were dispersed in ethanol and placed in a thoroughly cleaned quartz cuvette, with the baseline adjusted using blank ethanol. The experiment was conducted at a controlled room temperature of 25.0 ± 0.5°C. Measurements were performed three times, with the scanning light range set between 200 and 800 nm for better clarity (Rahman et al., 2024e).

### 3. Result and discussion

#### 3.1. FTIR-ATR analysis

The FTIR-ATR analysis has been accomplished to elucidate the presence of functional groups, molecular performance, chemical structure, chemical composition and so on (Sheikh et al., 2023). The analysis has demonstrated the upliftment of components corresponding to different treatment methods. The absorbance of the functional group and the elimination of lignin, and hemicellulose content from the raw fiber by sequential chemical treatment to obtain biopolysaccharide (CNC) are shown in Fig. 6. The aforementioned graph (Fig. 6.) dictates the circumstances of the raw fiber after several chemical treatments, i.e., Integrity of raw, alkali treated, bleached, and CNC has been performed

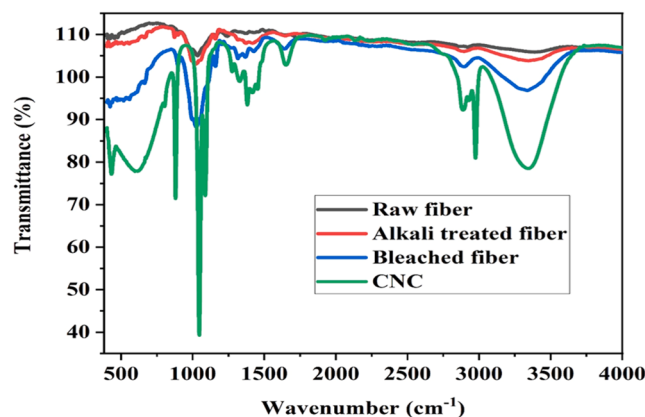


**Fig. 6.** Comparative FTIR spectrum of (a) RF, (b) ATF, (c) BF, and (d) CNC of maize shell in 400 to 4000  $\text{cm}^{-1}$  range.

through the test. The incorporation of probable and surprising functional groups, as well as their associated resonance, deformation, and bonding properties, is observed at specific wavelengths. The bonds responsible for absorption and the accounted groups associated with specified wavenumber have been charted in Table 2. The spectrum frequency ranges between 400 and 4000  $\text{cm}^{-1}$  and examines the peak with well-defined analogies by means of absorbance (Rahman et al., 2023d). The C—O—C symmetric stretching vibration in cellulose (Rahman et al., 2023a) has been assigned in raw fiber at about 1130  $\text{cm}^{-1}$ , C—H stretching at 2900  $\text{cm}^{-1}$  in alkanes, and -OH stretching at 3440–3490  $\text{cm}^{-1}$ , which develops points of interest in the graph. The observation of alkali-treated fiber shows that the peak of C—O—C vibration stretching has mostly been eliminated, which demonstrates that the treatment was accomplished successfully. In contrast, C—H stretching in alkanes remains in that position after several treatments, but peak intensity is elaborated more in response to its shifted its position, and -OH vibrational stretching has been sustained but slightly shifted to 3300–3400  $\text{cm}^{-1}$ , 3295–3510  $\text{cm}^{-1}$ , and 3320–3435  $\text{cm}^{-1}$  in raw, bleached fiber and CNC individually. The absorbance of alkali-treated fiber at 1140  $\text{cm}^{-1}$  implies that C—OH stretching of lignin content has been admirably eliminated after the bleaching operation, as shown in graphs where the peaks at this point are ascending progressively. According to the functional group, the clarity of peaks has been observed extensively after performing different elimination methods, where the functional groups are detected easily based on their stretching and bending properties. In the raw fiber, C—O and -OH stretching have been observed, which reveal tiny peaks. Subsequently, the graph's

intensity & sharpness have been increasingly extended by slightly shifting for the consecutive treatment method, due to the elimination of impurities and unwanted lignocellulosic materials (lignin, hemicellulose) respectively. The Symmetric bending of the  $\text{CH}_2$  group has been clearly observed in BF & has been extended after acid hydrolysis, indicating the presence of Cellulose that was not clearly observed in RF & ATF due to more impurities and hemicellulose content. An eye-catching (extended & sharp) graph of -C—O—C bending has been shown in CNC due to cellulosic rings that facilitate the breakdown of unit lignin (nano formation) from pure cellulose fiber, which was comparatively less in RF, ATF, & BF. The extensive peak in CNC ranges between 3320 and 3435  $\text{cm}^{-1}$ , implying -OH stretching of the hydroxyl ring, C—H stretching (Rahman et al., 2022; Rahman & Maniruzzaman, 2019) in alkane at 2930  $\text{cm}^{-1}$ , obtained by shifting from 2850 to 2900  $\text{cm}^{-1}$ , along with the appearance of new functional groups. The N—H stretching vibrational peak at 2975  $\text{cm}^{-1}$  indicates the existence of -NH<sub>2</sub> group, the -C—O—C bending vibration appeared due to cellulose ring, and the C—H symmetric bending vibration at 1400  $\text{cm}^{-1}$  is due to the accounted -CH<sub>2</sub> group. The shifted absorption C = O bond stretching at 1665  $\text{cm}^{-1}$  accounts for acids or esters groups, as well as numerous unknown function groups that appeared. Newly, appeared functional groups such as Si—O, C≡H stretching in alkaline, C = C—H str. vibration in alkene, S-H deformation (Rahman et al., 2023d), C≡N stretching, and organic C—Cl stretching have been shown in CNC at the wavelengths 450  $\text{cm}^{-1}$ , 2170  $\text{cm}^{-1}$ , 2710  $\text{cm}^{-1}$ , 2175  $\text{cm}^{-1}$ , and 625  $\text{cm}^{-1}$ , respectively. The bonds may be due to the origin of raw materials, the environment, or the applied chemical treatment methods. Throughout the successive treatment method, the redundant lignocellulose components were gradually eliminated, which can be observed in the graph by analyzing the characteristics of the specific compounds at defined wavelengths, i.e., C—O—C and C—OH stretching in alkali-treated as well as bleached fiber ranges around 1150–1220  $\text{cm}^{-1}$  peak. In the CNC absorbance graph, a linear peak implies mostly the elimination of lignin and hemicellulose content. In the FT-IR figure of maize shell, different functional groups are shown, and changes are induced after modifications, where -OH stretching displays in the 3120–3635  $\text{cm}^{-1}$  range, which indicates O—H bond stretching in the fiber. Subsequently, it gets sharper from RF, ATF, BF, and CNC after treatment, which demonstrates the elimination of hindering groups and other impurities that aid effective absorption. The RF peak shows C—H stretching with little intensity at 2850  $\text{cm}^{-1}$  and then gets sharper consecutively in ATF, BF, and CNC, where the CNC peak shifts slightly by evolving a neck-type short absorption. Another sharp peak evolved in CNC that was not observed in RF, ATF, and BF, which may be responsible for some chemical force of attraction. The RF shows a tiny broad peak at 1650  $\text{cm}^{-1}$  that is the same for ATF and shifts a while for BF as well as CNC by turning into a sharper

**Table 2**

Responsible functional group of chemically treated fiber with their respective wavenumber shown by FTIR analysis.

Adsorption bond	Accounted group	Raw fiber Peak ( $\text{cm}^{-1}$ )	Alkali treated fiber Peak ( $\text{cm}^{-1}$ )	Bleached fiber Peak ( $\text{cm}^{-1}$ )	CNC Peak ( $\text{cm}^{-1}$ )
-OH stretching	Hydroxyl ring	3440–3490	3300–3400	3295–3510	3320–3435
N-H stretching	Amines	.....	.....	.....	2975
C≡C stretching	Alkyne	....	....	....	2170
C = C-H str	Alkene	....	....	....	2710
C = O str	Acids or Esters	1650	1650	1660	1665
-C—O—C bending	cellulose ring	1030	1015	1030	1040
C-H symmetric bending	-CH <sub>2</sub>	....	....	1300	1400
C-C stretching	Styrene ring	1375	1425–1460	1450	1375
S-H deformation	....	....	....	....	2550
C-OH	Lignin ring	1140	1170	....	....
C-C	Alkane	....	1230	1200	-
C≡N str	Nitriles	....	....	....	2175
C-H str	Alkane	2900	2850	2850	2930
-OH out of plane	Hydroxyl	....	875	890	875
C-Cl str.	Organic chloride	....	....	....	625
Si-O	Inorganic	....	....	425	450

peak, which determines the presence of acid or ester functional groups by revealing C = O stretching that displays more clarity after modification. A neck vibration occurs in the 1375–1460 cm<sup>-1</sup> range due to the presence of a styrene ring by revealing C—C stretching. The symmetric -C—O—C stretching vibration of the cellulosic ring displays in RF at 1030 cm<sup>-1</sup> and is shifted slightly next by revealing an extended sharper peak in ATF, BF, and CNC, which determines the clarity of cellulose by eliminating hemicellulose, lignin, and other impurities respectively. RF contains lignocellulosic materials (cellulose, hemicellulose, lignin) and other impurities, where there should be rigorous intermolecular forces, i.e., van der Waals forces, hydrogen bonding, electrostatic forces, etc., in which the position and intensity of C—H and O—H bond stretching display changes in hydrogen bonding. Elsewhere, CNC imparts intramolecular forces and crystalline form by reducing the amorphous region, besides failure of intermolecular forces. The successive chemical treatments, such as alkali treatment and bleaching, eliminate the hemicellulose and lignin content from the fiber and concentrate cellulosic content by breaking down the aromatic and ester bonds, respectively. A few numbers of chemical groups are induced in CNC after several consecutive chemical treatment processes where some major organic/inorganic groups have been taken into consideration according to their bending & stretching nature (Arman et al., 2024). Hence, Inorganic Si-O adsorption bonds induced in CNC, which might have originated from the soil or air, as well as C—Cl stretching, could have been induced due to the presence of impurities of treatment chemicals. -C—O—C bending of Cellulose ring has been induced in CNC, which was not observed before acid hydrolysis, and C—H symmetric bending induced in CNC, along with a broad sharp graph of C—O stretching and a wide picture of -OH stretching, have been observed in the CNC graph compared to others, which implies that the elimination of unwanted materials in the CNC (i.e., Lignin, Hemicellulose, & other impurities) has occurred. Eventually, it can be emphasized that the FTIR-ATR analysis of maize fiber through isolated chemical treatment to demonstrate the purity of specimens and observe the presence of several functional groups has been performed effectively. The CNC graph displays that some functional groups have shifted from their preceding positions obtained after chemical treatment and may incorporate some surprising functional groups, as observed by their deformation at specified wavenumber that may appear during treatment. (Table 3)

### 3.2. FESEM analysis

FESEM analysis has been conducted to distinguish the surface morphology of maize shell fiber after passing through several chemical treatment processes by exposure to higher magnification (Rahman et al., 2018a; Sheikh et al., 2023). The FESEM image of the raw maize shell in Fig. 7(a) reveals that impurities (crystals) with oily and waxy substances were present on the heterogeneous surface of the raw fiber. The raw fiber surface demonstrated that before any chemical treatment, there were no intercellular gaps among fibrils, which indicates that the surface

was completely compacted and also articulates the presence of impurities, hemicellulose, lignin, cellulose, and waxy matter. The FESEM image in Fig. 7(b) revealed the surface attributes of raw fiber after alkali treatment, which distinguishes the condition of fiber after alkali treatment compared to the raw fiber. The image demonstrates that rough surfaces with numerous holes had developed. Raw fiber essentially consists of hemicellulose, cellulose, and lignin content; to extract crystalline nanocellulose (CNC), only cellulose is required; the other compounds should have been eliminated. The FESEM image of alkali-treated fiber determined that a single fiber detached from the bundle, compressing fibril diameter, which revealed that the impurities and hemicellulose content had been eliminated significantly. Eventually, it concludes that crystals and other impurities with hemicellulose have been removed, and the size reduction and genesis of single fiber complying with the treatment have been accomplished effectively. Fig. 7(c) disclosed the FESEM image of maize shell fiber after the bleaching operation. Compared to raw fiber, it can be inferred from the image that the impurities, fatty, and waxy substances have been removed thoroughly. The image also implies that a uniform surface and intermolecular gaps have appeared to a great extent, which distinguishes explicitly between raw and bleached FESEM images. Lignin, hemicellulose, cellulose, and other impurities bind raw fiber; that's why there is less exposure to COOH and -OH groups contained in cellulose. By conducting a bleaching operation, individual microfibrils along with functional groups have been exposed, which determined that the hemicellulose, and lignin have disappeared effectively (Rahman & Maniruzzaman, 2024).

When the particle size of cellulose exhibits in the nano range (i.e., below 100 nm), it is termed crystalline nanocellulose (CNC) (Deng et al., 2016). The surface morphology and dimension of CNC were analyzed through the FESEM images. Additionally, the particle size of the final CNC was measured using ImageJ software. In Fig. 7(d), the FESEM image of CNC is displayed, where the characteristic and conditions of the surface are enlarged in comparison with the FESEM images of raw shell fiber. The transparent FESEM image of CNC elaborates that the lignin, hemicellulose, and impurities have been completely eliminated. The FESEM image of CNC illustrates the enrichment of rough surfaces and microporous holes, where honeycomb-like structures with a uniform pore size (uniform distribution) were identified. The uniform distribution implies uniform porosity (holes), shape (honeycomb-like microstructure), and small particle size that have been observed throughout the surface with tiny differences, which reveal perfect microstructure forms by increasing the surface area. A uniform distribution of particles has been observed throughout the surface, which implies uniform porosity (holes), a spherical shape (honeycomb-like microstructure), and small particle size with tiny differences that reveal perfect microstructure forms by increasing the surface area. The honeycomb-like microstructure and uniform size distribution on the surface can enhance solubility, dissolution rate, and the formation of a homogeneous mixture in the drug. The drug delivery systems follow different conditional characteristics such as physical, chemical, and morphological properties, besides polarity and bonding interactions, which enhance the sustainable release of the drug as a bridge between CNC and the drug by increasing the surface area and porosity, which are directly correlated with shape (Patra et al., 2018). As the particle size increases, the surface area decreases, revealing lower permeability that is susceptible to a slower digestion rate of the drug. CNC extracted from maize shell could be beneficially applicable in wastewater treatment as a Composite (constructed with CNC and carbonous molecules using a suitable treatment method), where a honeycomb-like microstructure and uniform size distribution on the surface enhances CNC's effectiveness by absorbing heavy metal & trace elements in the holes of the composite surface. Unit lignin has been detached and generated microfibrils that demonstrate that the dimension was significantly reduced to a nanoscale. Histogram analysis (distribution curve) using ImageJ software showed in Fig. 9 that the particle diameter is below 200 nm,

**Table 3**

Mass loss, reaction mode, and degradation rate of different chemically treated fiber using TGA, DTA, and DTG thermal analysis.

Parameters	Raw fiber (% at °C)	Alkali treated fiber (% at °C)	Bleached fiber (% at °C)	CNC (% at °C)
Initial loss	10.8 at 263	10 at 280	8.5 at 252	9 at 275
Maximum loss	84 at 600	80 at 600	92.5 at 600	64 at 600
50 % degradation	348 °C	360 °C	345 °C	370 °C
Highest degradation	276 °C	315 °C	288 °C	285 °C
Residue at 600 °C	16 %	20 %	7.5 %	36 %
Endothermic peaks at °C	90, 362	110, 378	90, 152	95, 355, 513
Maximum rate of mass loss (μg/min)	1048	910	1575	590

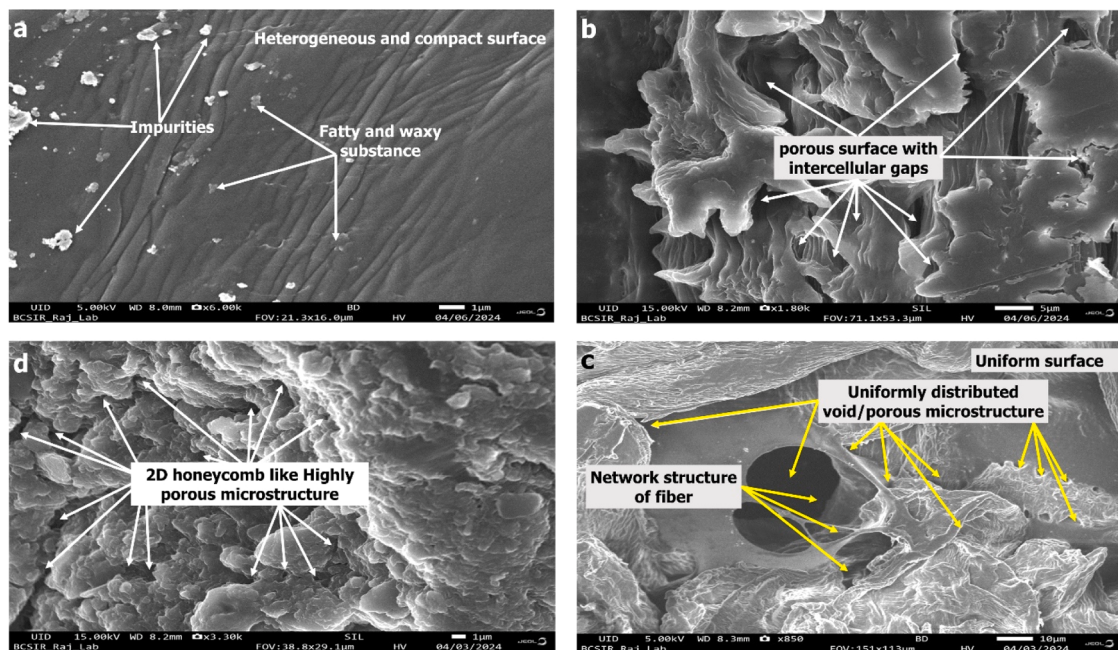


**Fig. 7.** Comprehensive FESEM image of maize shell's (a) RF, (b) ATF, (c) BF, and (d) CNC under 850x to 6000x magnification range after several chemical treatments.

with the maximum particle size found in the 0–65 nm range. Subsequently, the analysis elaborated that CNC extraction from maize shell fiber was lowered to the nano range (below 100 nm), which indicates that the experiment was performed successfully.

### 3.3. EDX analysis

EDX analysis has been performed to detect molecules and their composition on the surface of raw fiber, alkali treated fiber, bleached

fiber, and CNC specimens. Energy Dispersive X-ray spectroscopy (EDS) of the subjected specimens has been presented in Figs. 8(a-d). Fig. 8(a) reveals that the elements C (39.83 %) and O (59.18 %) are present in the raw fiber. Fig. 8(b) shows that C (40.62 %), and O (58.51 %) are present in alkali treated fiber. In Fig. 8(c), C (40.16 %), and O (59.84 %) molecules were present in bleached fiber. In Fig. 8(d), EDS analysis of CNC revealed that C (47.9 %) and O (40.38 %) molecules were present. Some elements were eliminated and incorporated after the chemical treatment process, which can be described by the observation. The spectrum

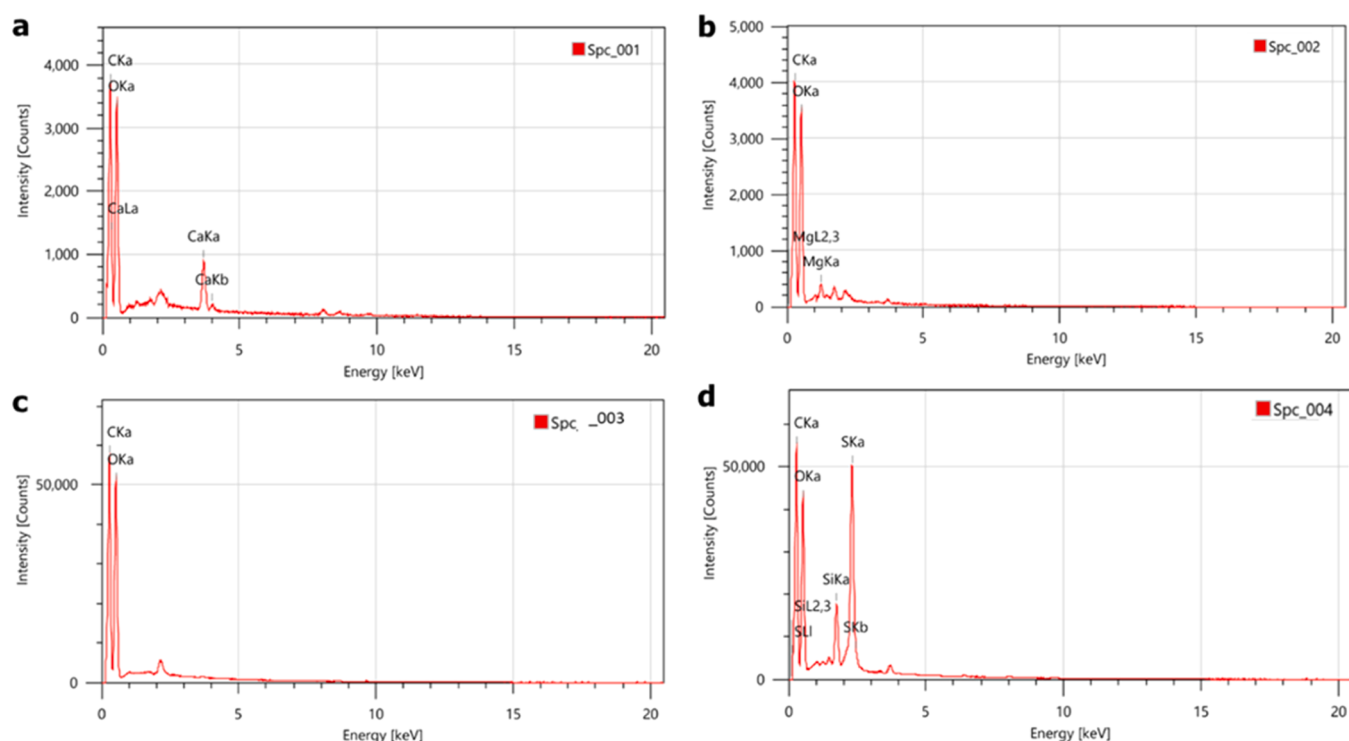


**Fig. 8.** Energy Dispersive X-ray spectrum of (a) RF (b) ATF, (c) BF, and (d) CNC for elemental analysis.

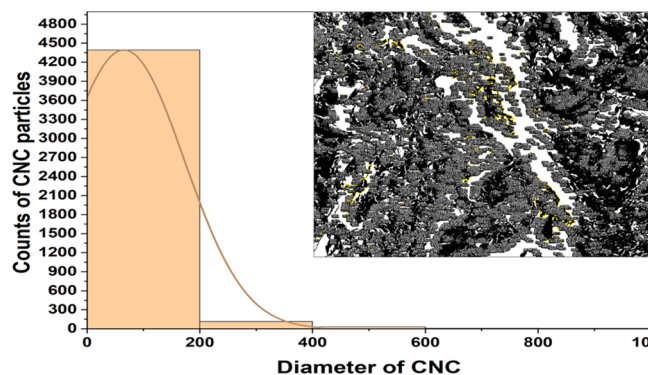


**Fig. 9.** Size distribution curve (histogram) of CNC extracted from secondary plant (maize shell) fiber with the help of ImageJ software and Origin lab software by manipulating FESEM.

analysis through EDS exhibits that C and O molecules are present in each specimen, and besides these, some elements were found at trace levels, such as Mg, Ca, Si, and S. In Fig. 8(d), a newly appeared elevated sharp peak demonstrates the presence of Sulphur (S), which can be originated from  $\text{SO}_4^{2-}$  group during hydrolysis process. The negatively charged sulphate group can effectively interact with positively charged heavy metals in the water purification process, which implies the accuracy and effectiveness of the extracted CNC enhancement.

#### 3.4. Thermal profile analysis

##### 3.4.1. TGA analysis

The development of polymeric composite is extensively relatable to the thermal degradation subjected to during processing, where the thermal properties (materials stability, less organoleptic, and moisture loss) of polymeric/biopolymeric samples can be analyzed by the thermogravimetric analysis (Izani et al., 2013). The samples (raw fiber, alkali treated fiber, bleached fiber, and CNC) had been subjected to controlled heating to observe the mass loss against temperature at a specified rate, where volatile components, lignocellulosic constituent (cellulose, hemicellulose and lignin), impurities, and amount of moisture dictates the deterioration consequence of biopolymeric sample in several phases (three region) by exploiting temperature ranges between 25 °C and 600 °C, which can vary based on the origin and types of polymeric/biopolymeric fibers to identify thermal stability (Rahman et al., 2024f). Fig. 10 exhibits the moisture loss curve against a range of heat applied at a specified rate for several chemically treated fibers. The degradation can appear due to elimination (breakdown functional bonds) of functional groups in response to heat, involving two or more

steps. The raw fiber in Fig. 10 began to lose weight at 50 °C and transitioned up to 130 °C, where a tertial transition sustained at 265 °C to 385 °C due to vaporizing water or high volatile compounds from the sample. As the degradation takes place, several steps are observed, where the primary decomposition was noted in the amorphous region, ranging between 50 °C to 265 °C.

The chemical degradation through alkali treatment (eliminating hemicellulose which began to rapidly decompose at 282 °C) had increased thermal stability of the fiber. After that, the alkali-treated fiber exhibited unfamiliar behavior due to the supplementary decomposition of the Pyranose ring, making it identifiably stable. By the bleaching operation (which removed lignin content) of the fiber, the crystallinity index had increased due to a reduced loss of moisture content; consequently, thermal stability of materials increased in the secondary phase of degradation. In the secondary phase analysis, the thermal stability of CNC has increased due to less mass loss and a uniform structure (high Charbonneau's residue in CNC and minor Charbonneau's residue associated with raw fiber that indicates the elimination of lignocellulosic contents, i.e., lignin, hemicellulose) of biopolymeric fiber, which exhibited high thermal compatibility at 600 °C compared to other chemical treatment operations. Subsequently, it can be concluded from the thermogravimetric analysis that the thermal stability of CNC is far more compatible and beneficial for use in materials manufacturing.

##### 3.4.2. DTA analysis

The thermal behavior and treatment consequences from RF to CNC can be analyzed by DTA. In the Fig. 11, a DTA graph of raw fiber, alkali treated fiber, bleached fiber, and CNC is exhibited, showing the changes induced on the thermogram as a series of chemical treatment correspond to the applied heat. As the RF contains moisture, lignocellulosic materials, and other impurities, the elimination of these materials by chemical treatments to obtain CNC has been observed through thermal degradation. RF, ATF, and BF shows an endothermic reaction at the initial stage below 100 °C, which later extends, revealing the evaporation of loosely bonded water molecules and volatile components from the surface of biomass. The thermal breakdown of hemicellulose is observed by the intermediate endothermic peak of ATF at 370 °C. Later, an exothermic peak is induced in BF at 362 °C, which extends up to 450 °C due to the oxidation (release heat) of pyranose ring from lignin during the degradation of molecules, implying the existence of residual homogeneous materials by removing other contents from the fiber. The CNC shows a tiny endothermic peak below 100 °C and a single intermediate exothermic peak at 320 °C, indicating a loss of moisture and oxidative breakdown of some lignin contents that were present in small amount at comparatively lower temperatures, respectively. As the non-cellulosic species have been removed from CNC, the thermal stability and clarity of cellulose increased, which is suitable for various application. Eventually, DTA results helps to determine the precision of the

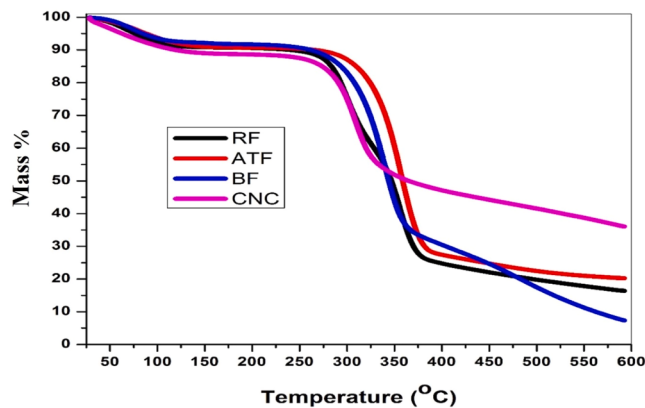


**Fig. 10.** Thermal stability of subjected different treated polymeric (a) RF, (b) ATF, (c) BF, and (d) CNC samples.

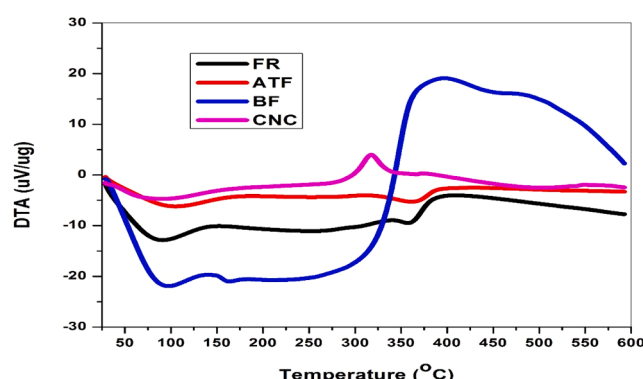


**Fig. 11.** Reaction mode analysis using DTA curve of different chemically treated fibers.

obtained CNC.

#### 3.4.3. DTG analysis

The DTG curve demonstrates the mass loss per minute subjected to heat employed on the polymeric specimen. Fig. 12 exhibits mass loss rate of raw fiber (RF), alkali treated fiber (ATF), bleached fiber (BF), and CNC samples correspond to temperature variance. The raw polymeric/biopolymeric fiber basically consists of cellulose, hemicellulose, lignin and ash (impurities) contents. Numerous chemical treatments had been accomplished to enhance the materials strength and susceptibility by exposing it to heat. The peaks were observed in different regions based on the attributes of the material's composition (Gupta et al., 2023). In Fig. 12, each fiber (raw and chemically treated) exhibited the same behavior below 100 °C, which contributes to the evaporation of moisture. The raw fiber displays mass loss of about 1048 µg/min at 358 °C due to the eradication volatile compounds. The mass loss transpires in the amorphous region, with temperature ranges between 250 and 400 °C, where loosely bonded compounds degrade readily due to exposure to heat. The degradation of hemicellulose from alkali-treated fiber exhibits a mass loss of 910 µg/min at 358 °C. In the case of bleached fiber, mass loss appeared at 1565 µg/min at 337 °C, which indicates that at this temperature, more mass loss occurs due to the removal of lignin content by bleaching, along with further mass loss of about 207 µg/min at 475 °C due to the decomposition of pyranose ring, which may indicate the presence of some hemicellulose content. Subsequently, moisture loss in CNC shows comparatively low values, about 590 µg/min at 312 °C. In the DTG against temperature curves, the RF shows two TG because RF contains cellulose, hemicellulose, lignin, etc., as specific constituents degrade at specific temperatures. Here, the first peak around 300° is due to the degradation of the hemicellulose-based composition, and the second peak is due to the degradation of the cellulosic component existing in the RF. That's why the total degradation results in three broad peaks, including moisture loss. Consequently, the observation implies that mass loss in CNC is comparatively much lower than that in raw fiber, alkali-treated fiber, & bleached fiber, which revealed more uniformity of fiber and successfully compiles the elimination of hemicellulose, and lignin contents. Noteworthy from the above discussion, it can be said that as the mass loss is considerably less, thus the thermal stability and purity of CNC are more precise, which obeys the materials that are more susceptible to heat, as well as it could be beneficially used in materials fabrication and nano-composite formation (Rahman et al., 2024c). Therefore, the analysis complies with the aforementioned discussion precisely.

#### 3.5. XRD analysis

The polymeric/biopolymeric fiber contains amorphous and

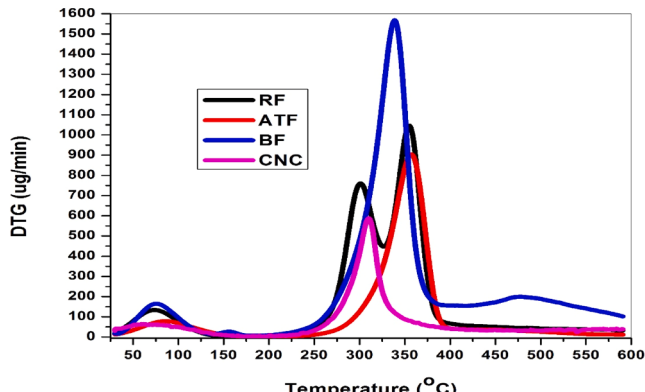


Fig. 12. Degradation rate of (a) RF, (b) ATF, (c) BF, and (d) CNC of maize shell using DTG analysis.

crystalline regions as well as defects. To distinguish fiber crystalline behavior (crystalline index,  $C_{RI}$ ), significant modification (successive chemical treatments) can be observed through XRD analysis (Sampath et al., 2017). The XRD analysis of raw fiber, alkali-treated fiber, bleached fiber, and CNC specimens is displayed in Fig. 13, where the  $2\theta = 21.89^\circ$  exhibits (200) crystallographic plane (Sampath et al., 2017; Zhao et al., 2019). In an ideal crystal, the peak width will be negligible and there will be sharp peaks at different points corresponding to the planes of materials, where an extensive sharp peak specifies enhancement of crystallinity, which illustrates the purity of cellulosic fiber (Tavana et al., 2024). In the (200) crystallographic plane, an identical broad peak is shown in the XRD graph of each sample (RF, ATF, BF, CNC) that dictates a clear peak intensity at  $2\theta = 21.89$ , where RF shows a widened peak at  $2\theta = 16-22.5$ , which reveals the existence of lignocellulosic materials as well as impurities, causing the sharpness of RF peak to decrease with increasing width. Later, these materials have been eliminated by several chemical treatment methods, increasing the peak sharpness (increase the purity of fiber) respectively. Hence, the peak intensity has increased in the ATF graph by eliminating hemicellulose from the raw fiber. Subsequently, the peak width has decreased, and a sharper peak arises in BF by eliminating lignin content and impurities. Afterward, an extended sharp peak has arisen in the CNC graph, indicating that the crystallinity of fiber increases prominently, revealing a pure CNC formulation (de Moraes Teixeira et al., 2010). Noteworthy is that some tiny crystal peaks have been identified in CNC, which might be potential contaminants. Although they are much smaller in size, they determine that CNC contains a few ordered structures. The crystallinity index of different chemically treated shell fibers has been tabulated in Table 4. While the crystallinity index value of RF, ATF, BF, CNC were found around  $36.01 \pm 0.09\%$ ,  $44.15 \pm 0.19\%$ ,  $57.55 \pm 0.15\%$ , and  $76.09 \pm 0.91\%$  respectively (after performing the baseline correction). Consequently, the XRD analysis revealed that the crystallinity index has been increased by precise modifications where the crystallinity index of CNC increased significantly to about  $(76.09 \pm 0.91)\%$  compared to raw fiber ( $36.01 \pm 0.09\%$ ), which implies that the morphological property of CNC is implausible: with these features, it can be beneficial for industrial application. The average of trials ( $n = 3$ ) of crystallinity index  $\pm SD$  (standard deviation) has been assessed in Table 4, to regulate the behavior of the subjected different polymeric samples with considered  $\pm 5\%$  integrity. CNCs obtained from maize shell reveal several significant properties, i.e., highly porous honeycomb-like microstructure, extensive thermal stability (showing high residual mass at 600°C), high yields, and desired crystallinity which have a JCPDS-ICDD card number (00-056-1718). Thus, they can be applied beneficially in automotive

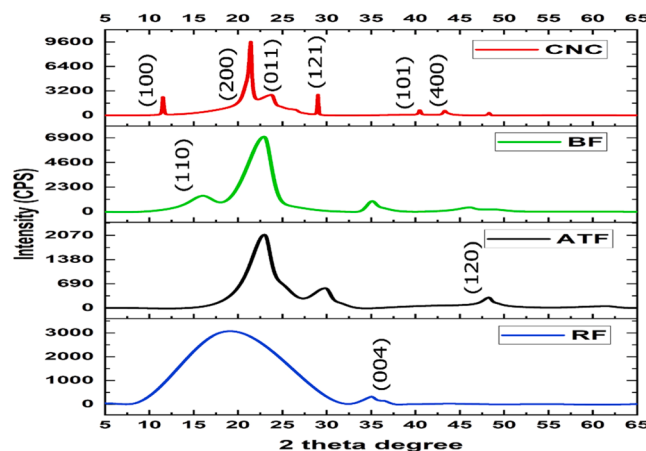


Fig. 13. Comparative crystallinity index (calculated and plotted with baseline correction) of (a) RF, (b) ATF, (c) BF, and (d) CNC specimens by exploiting 2 theta range 5 to 70° with respect to their crystalline plane as counts per second (CPS).

**Table 4**

Crystallinity index values (calculated and plotted with baseline correction) of different chemically treated fiber in this study.

Samples	CrI ± SD (%)
Raw Fiber	36.01±0.09
Alkali treated fiber	44.15±0.19
Bleached fiber	57.55±0.15
CNC	76.09±0.91

Here, the number of trials ( $n = 3$ ), and the values are presented in Table 4 as mean ± standard deviation (SD). Which has been statistically analyzed by analysis of variance (ANOVA) to estimate the properties of the sample meaningfully different at the level of 5 % (Probability,  $p < 0.05$ ).

sectors prone to high temperatures due to their high residual mass at extensive temperatures compared to others. A typical comparison among CNCs extracted from different cellulosic secondary plant sources is displayed in Table 5.

### 3.6. Particle size and zeta potential analysis

The diameter of the extracted CNC particles is shown in Fig. 14(a), which displays that the average particles are observed to be below 150 nm. The Zeta potential of the extracted CNC has been analyzed by dynamic light scattering, as shown in Fig. 14(b), which ranges -500 to 500 mV, revealing a high intensity at -1.4 mV. This demonstrates that the particles present at the surface were negatively charged, which could be responsible for the magnificent stability in the colloidal system due to repelling each other in the dispersion medium (Asadi et al., 2022). Zeta potential measures the surface charge of molecules, which affects the dispersion of CNC in nonaqueous suspension and develops the carriage of lysosome to cells through endocytosis, i.e., overcoming the defensive barrier in the drug-loaded system (Arshad et al., 2024). Particle solubility, permeability, drag degradation, drug delivery system (i.e., oral release), and capacity for action at the targeted site are strongly affected by the surface charge (i.e., either negative or positive). The drag delivery systems follow different conditional characteristics such as physical, chemical, and morphological properties, besides polarity and bonding interactions, which enhance the sustainable release of the drug as a breach between CNC and the drug (Patra et al., 2018). The surface charge of the colloidal medium affects the size distribution of CNC throughout the solution (associated with the formation of a homogeneous mixture in the drug) that is accompanied by a physical agent in drug nano-formulation, which can be analyzed through zeta potential. The physical agents are concentration, pH, electrolytes and so on, where zeta potential analysis is crucial for suitable drug delivery, as the surface charge of CNC can affect the iontophoretic flux and drug concentration (shows a linear relationship) which can help drug delivery via nanocarriers, allowing drugs to penetrate the skin subsequently spread to the

**Table 5**

A comparative study of the CNCs extracted from different cellulosic secondary plant sources based on TGA (residual mass) and crystalline index analysis.

Source	Residual mass (%) at 600°C	Crystallinity Index (%)	Reference
Keya leaf	37.00	61.31	(Hossain et al., 2024)
Maize cob	38.00	84.63	(Dewan et al., 2024)
Rice straw	35.40	76.00	(Thakur et al., 2020)
Okra stalks	35.05	86.09	(Rahman et al., 2024b)
Sugarcane leaf sheath	36.00	81.89	(Hassan et al., 2024)
Maize shell	40.00	76.09	This study

targeted tissues. Additionally, changing the pH of the solution can modify ionization or net charge. These modifications can be performed by the analyzing the CNC surface charge through zeta potential analysis (Sharma, 2019). (Fig. 15)

### 3.7. UV–Vis–NIR analysis

Organic compounds show a distinguished pattern of UV spectrum that can indicate their presence and purity in the examined matrix. The prepared maize shell-derived CNC was finally preserved in a solution of ethanol where it existed as a suspension. The suspension of maize shell-derived CNC was diluted with absolute ethanol and placed in the cuvette of the UV chamber to examine the spectral pattern in the UV–Vis–NIR wavelength (200–800 nm) range. From the spectrum (in Fig. 15), it is observed that the wavelength range of 380–800 nm is free of any absorption peaks indicating the absence of coloring and chromophoric functional groups in the sample matrix. Hence, the prepared CNC did not contain any pigments and lignin-based compounds indeed (Hossain et al., 2024). The produced CNC is lignin-free as well as semitransparent, indicating that the alkali treatment and bleaching operations were effective during the isolation period. On the other hand, a broad absorption peak is noticed in the 230–290 nm range, which is characteristic of glucopyranose units of cellulose (Hassan et al., 2024). A higher absorbance was observed at shorter wavelengths by the UV–Vis–NIR analysis, which may be due to accumulation (improper dispersion), mismatch, or light scattering effects of CNC with the solvent. Based on these observations, it can be claimed that the preparation methodology followed in that research is adequate enough to produce high-quality CNC from such type of solid agro-waste source as maize shell. Similar UV–Vis–NIR spectra have been noticed previously in the literature, where cellulosic units showed distinguished patterns in that wavelength range, which may be due to the bandgap between the highest occupied molecular orbital and lowest unoccupied molecular orbitals of the respective glucopyranose repeat units of CNC (Rahman et al., 2024e).

### 4. Conclusion

In this study, a new method for the production of CNC from a very new and beneficial source, namely *Zea Mays*, was performed through successive chemical treatments, i.e., alkali treatment, bleaching, and acid hydrolysis. The physical and morphological properties of fibers at different modification steps have been successfully analyzed using FTIR, FESEM, EDX, DLS, TGA, and XRD analyses to clarify the functional properties, surface morphology, particle size, reaction mode, and potential change of CNC. Hence, the FTIR-ATR analysis displayed bond stretching (-OH, C–H, C = O) along with bending (-C–O–C) and less vibrational noise in the CNC, which demonstrates the exposure of numerous functional groups at specified wavenumbers. The FESEM analysis disclosed a clear observation of the treatment effect on the fiber by exposing a smooth fiber surface and numerous microporous holes, along with a 2D honeycomb-like microstructure in CNC. The thermal stability of CNC was exceptionally high (40 % residue at 600 °C) compared to others, as observed in the TGA analysis, which revealed that the thermal stability of CNC had been significantly increased by chemical treatment. ATF eliminates hemicellulose and other impurities from raw fiber, increasing the cellulose content of the fiber, which enhances thermal stability, tensile strength, and surface morphology compared to RF. Thus, it can be applied in several fields, including household materials, packaging materials, and so on. The bleaching of ATF removes bundle lignin and reveals highly pure, soft, and white cellulose fiber with an extended surface area and thermal stability; thus, it can be applied in the paper industry (writing and printing paper), in making microfilter membranes, and in textiles where yellowing is not desired. CNC is the most desirable product of RF that has an extended field of application where extensive thermal stability is required. CNC can be applied in numerous sectors, such as making composites by

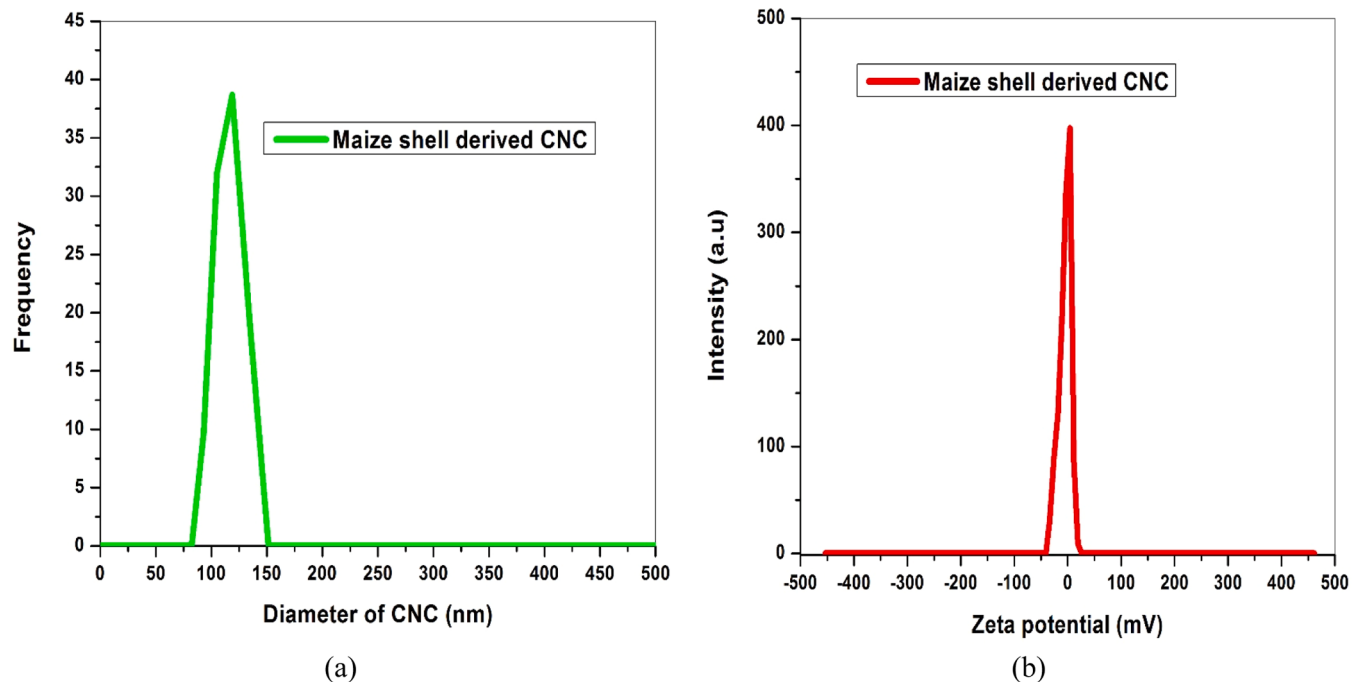


**Fig. 14.** Observed (a) diameter, and (b) zeta potential of the newly extracted CNC by exploiting ranges 0 to 500 nm and  $-500$  to  $500$  mV respectively using dynamic light scattering (DLS) analysis by conducting particle size analyzer while a.u stands for an arithmetic unit.

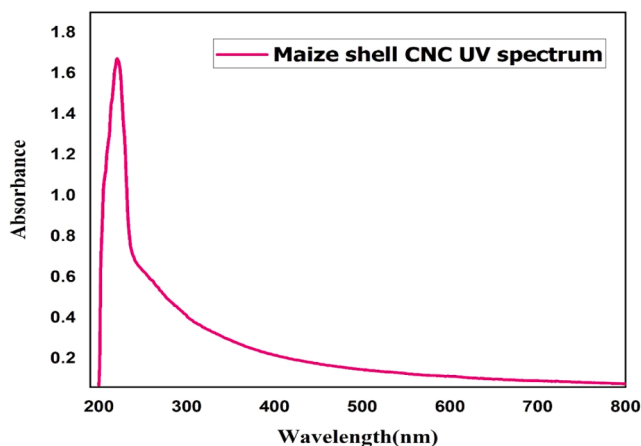


**Fig. 15.** UV-Vis-NIR analysis of maize shell derived semitransparent CNC suspension in the range of 200 nm to 800 nm wavelength.

combining it with other materials for its honeycomb-like uniform microstructure and extended surface area, including drug delivery (pharmaceutical nano formulation), car body parts, and electronic components, revealing enormous thermal stability in hostile environments up to  $600^{\circ}\text{C}$ . The XRD analysis displayed that the crystallinity index of CNC is  $76.09 \pm 0.91\%$ , which is far higher than that of raw fiber ( $36.01 \pm 0.09\%$ ), revealing that the purity and morphological properties of CNC are incredible. The smaller particle size (below 100 nm) of the CNC was determined by the DLS method, which assessed the satisfactory development of nanoparticles from maize shells. Consequently, the aforementioned characterization study revealed that the CNC formulation performed successfully, highlighting the novelty of CNC production from a particular secondary plant fiber that was deemed agro-waste prior to the study, which exhibits excellent susceptibility to heat and striking mechanical properties. Due to these outstanding properties, the newly produced CNC could be beneficially used as a reinforcement agent to fabricate multifunctional bionanocomposites. Furthermore, this

would be used significantly in various sectors (such as wastewater treatment, electronics, and the automobile industry) as a suitable replacement for conventional fossil-based hazardous materials for sustainable environmental protection.

#### CRediT authorship contribution statement

**M Mohinur Rahman Rabby:** Writing – original draft, Resources, Methodology, Data curation. **Md.Mahmudur Rahman:** Writing – review & editing, Writing – original draft, Validation, Supervision, Software, Resources, Project administration, Methodology, Investigation, Funding acquisition, Formal analysis, Data curation, Conceptualization. **Bijoy Chandra Ghos:** Visualization, Methodology, Formal analysis. **Md. Abdul Gafur:** Visualization, Software. **Md. Al-Amin:** Software, Resources. **Shamim Dewan:** Methodology, Investigation. **Md.Ashraful Alam:** Validation, Software. **Md.Ismail Hossain:** Writing – review & editing, Methodology, Formal analysis, Data curation.

#### Declaration of competing interest

The authors declare that they have no known competing financial interests or personal relationships that could have appeared to influence the work reported in this paper.

#### Acknowledgment

All authors of this paper devoutly acknowledge the chairman of Bangladesh Council of Scientific and Industrial Research (BCSIR), Director of BCSIR Rajshahi Laboratory as well as the Ministry of Science and Technology (MOST), People's Republic of Bangladesh for their financial support and for consenting us to conduct their highly sophisticated instruments for experimentation. Furthermore, I want to acknowledge my parents (Md. Mokhlasur Rahman and Mrs. Rousonara) and my better half Suraiya Naznin, along with my attendant Md. Mofuj Islam for their encouragement and cordial support during the experimental session and drafting. Moreover, this work is sincerely dedicated to the memory of the martyrs including Al Mukaddas and Md. Waliullah

from Islamic University who were concealed by the autocratic government of Bangladesh as well as Abu Sayed, Mir Mahfuzur Rahman Mugdho, Ali Rayhan and many others of the July-August revolution (2nd liberation of Bangladesh) who were killed by the autocratic government.

## Funding

The authors extend their appreciation to the Ministry of Science and Technology (MOST), the People's Republic of Bangladesh, and the Bangladesh Council of Scientific and Industrial Research (BCSIR), for their joint funding to conduct this current work through Research and Development Project under grant number of (G.O.39.00.0000.01 2.02.009.23.159 and G.O. 39.02.0000.011.14.169.2023/877).

## Data availability

Data will be made available on request.

## References

- Adil, S. F., Bhat, V. S., Batoo, K. M., Imran, A., Assal, M. E., Madhusudhan, B., et al. (2020). Isolation and characterization of nanocrystalline cellulose from flaxseed Hull: A future onco-drug delivery agent. *Journal of Saudi Chemical Society*, 24, 374–379. <https://doi.org/10.1016/j.jscs.2020.03.002>
- Adnan, K. M. M., Sarker, S. A., Tama, R. A. Z., & Pooja, P. (2021). Profit efficiency and influencing factors for the inefficiency of maize production in Bangladesh. *Journal of Agriculture and Food Research*, 5, Article 100161. <https://doi.org/10.1016/J.JAFR.2021.100161>
- Almeida, A. P. C., Canejo, J. P., Fernandes, S. N., Echeverria, C., Almeida, P. L., & Godinho, M. H. (2018). Cellulose-based biomimetics and their applications. *Advanced Materials*, 30, Article 1703655. <https://doi.org/10.1002/ADMA.201703655>
- Amiri, A., Triplett, Z., Moreira, A., Brezinka, N., Alcock, M., & Ulven, C. A. (2017). Standard density measurement method development for flax fiber. *Industrial Crops and Products*, 96, 196–202. <https://doi.org/10.1016/J.INDCROP.2016.11.060>
- Arman, S., Hadavi, M., Rezvani-Noghani, A., Bakhtparvar, A., Fotouhi, M., Farhang, A., Mokaberi, P., Taheri, R., & Chamani, J. (2024). Cellulose nanocrystals from celery stalk as quercetin scaffolds: A novel perspective of human holo-transferrin adsorption and digestion behaviours. *Luminescence*, 39, e4634. <https://doi.org/10.1002/BIO.4634>
- Arshad, A., Arshad, S., Alamgeer, Mahmood, A., Hussain Asim, M., Ijaz, M., Muhammad Irfan, H., Rubab, M., Ali, S., & Raza Hashmi, A. (2024). Zeta potential changing self-nanoemulsifying drug delivery systems: A newfangled approach for enhancing oral bioavailability of poorly soluble drugs. *International Journal of Pharmaceutics*, 655, Article 123998. <https://doi.org/10.1016/J.IJPHARM.2024.123998>
- Asadi, A., Gholami, F., & Zinatizadeh, A. A. (2022). Enhanced oil removal from a real polymer production plant by cellulose nanocrystals-serine incorporated polyethersulfone ultrafiltration membrane. *Environmental Science and Pollution Research*, 29, 37144–37158. <https://doi.org/10.1007/S11356-021-18055-4>
- Baltazar-y-Jimenez, A., & Bismarck, A. (2007). Wetting behaviour, moisture up-take and electrokinetic properties of lignocellulosic fibres. *Cellulose*, 14, 115–127. <https://doi.org/10.1007/S10570-006-9092-X> METRICS
- Bhattacharjee, S. (2016). DLS and zeta potential – What they are and what they are not? *Journal of Controlled Release*, 235, 337–351. <https://doi.org/10.1016/J.JCONREL.2016.06.017>
- Blanco, A., Monte, M.C., Campano, C., Balea, A., Merayo, N., Negro, C., 2018. Nanocellulose for Industrial Use: Cellulose Nanofibers (CNF), Cellulose Nanocrystals (CNC), and Bacterial Cellulose (BC). Handbook of Nanomaterials for Industrial Applications. 74–126. <https://doi.org/10.1016/B978-0-12-813351-4.00005-5>.
- Bunaciu, A. A., Udrîștioiu, E.gabriela, & Aboul-Enein, H. Y. (2015). X-Ray Diffraction: Instrumentation and Applications. *Critical Reviews in Analytical Chemistry*, 45, 289–299. <https://doi.org/10.1080/10408347.2014.949616>
- Coseri, S. (2017). Cellulose: To depolymerize... or not to? *Biotechnology Advances*, 35, 251–266. <https://doi.org/10.1016/J.BIOTECHADV.2017.01.002>
- Datta, S., Christena, L. R., & Rajaram, Y. R. S. (2012). Enzyme immobilization: An overview on techniques and support materials. *3 Biotech*, 3, 1. <https://doi.org/10.1007/S13205-012-0071-7>
- de Morais Teixeira, E., Corrêa, A. C., Manzoli, A., de Lima Leite, F., de Ribeiro Oliveira, C., & Mattoso, L. H. C. (2010). Cellulose nanofibers from white and naturally colored cotton fibers. *Cellulose*, 17, 595–606. <https://doi.org/10.1007/S10570-010-9403-0> METRICS
- Deng, H., Hu, X., Li, H. A., Luo, B., & Wang, W. (2016). Improved pore-structure characterization in shale formations with FESEM technique. *Journal of Natural Gas Science and Engineering*, 35, 309–319. <https://doi.org/10.1016/J.JNGSE.2016.08.063>
- Dewan, S., Rahman, Md. M., Hossain, Md. I., Ghos, B. C., Rabby, M. M. R., Gafur, Md. A., Al-Amin, Md., & Alam, Md. A. (2024). Isolation and characterization of CNC from waste maize cob available in Bangladesh as a potential candidate for the fabrication of multifunctional bio-nanocomposites: A new approach. *South African Journal of Chemical Engineering*. <https://doi.org/10.1016/J.SAJCE.2024.12.007>
- El Messaoudi, N., Miyah, Y., Georgin, J., Wasilewska, M., Felisardo, R. J. A., Mokadiri, H., Manzar, M. S., Aryee, A. A., Knani, S., & Rahman, M. M. (2024). Recent developments in the synthesis of tetraethylengenetamine-based nanocomposites to eliminate heavy metal pollutants from wastewater through adsorption. *Bioresource Technology Reports*, 28, Article 101982. <https://doi.org/10.1016/j.briteb.2024.101982>
- Erenstein, O., Jaleta, M., Sonder, K., Mottaleb, K., & Prasanna, B. M. (2022). Global maize production, consumption and trade: Trends and R&D implications. *Food Security*, 14(5), 1295–1319. <https://doi.org/10.1007/S12571-022-01288-7>
- Eyley, S., & Thielemans, W. (2014). Surface modification of cellulose nanocrystals. *Nanoscale*, 6, 7764–7779. <https://doi.org/10.1039/C4NR01756K>
- Fatfat, Z., Karam, M., Maatouk, B., Fahs, D., & Galí-Muñtasib, H. (2023). Nanoliposomes as safe and efficient drug delivery nanovesicles. *Advanced and Modern Approaches for Drug Delivery*, 159–197. <https://doi.org/10.1016/B978-0-323-91668-4.00002-2>
- Gupta, V., Ramakanth, D., Verma, C., Maji, P. K., & Gaikwad, K. K. (2023). Isolation and characterization of cellulose nanocrystals from amla (*Phyllanthus emblica*) pomace. *Biomass Conversion and Biorefinery*, 13, 15451–15462. <https://doi.org/10.1007/S13399-021-01852-9> METRICS
- Halden, R. U. (2010). Plastics and health risks. *Annual Review of Public Health*, 31, 179–194. <https://doi.org/10.1146/ANNUREV.PUBLHEALTH.012809.103714/CITE/REFWORKS>
- Hassan, M. M., Rahman, M. M., Ghos, B. C., Hossain, M. I., & Zuhane, M. K. A. (2024). Extraction, and Characterization of CNC from waste sugarcane leaf sheath as a reinforcement of multifunctional bio-nanocomposite material: A waste to wealth approach. *Carbon Trends*, 17, Article 100400. <https://doi.org/10.1016/j.cartre.2024.100400>
- Hossain, M. I., Rahman, M. M., Ghos, B. C., Gafur, M. A., Alam, M. A., & Rabbi, M. A. (2024). Preparation and characterization of crystalline nanocellulose from keya (*Pandanus tectorius*) L. fiber as potential reinforcement in sustainable bionanocomposite: A waste to wealth scheme. *Carbohydrate Polymer Technologies and Applications*, 8, Article 100600. <https://doi.org/10.1016/j.jcapta.2024.100600>
- Janeni, J., & Adassoorya, N. M. (2021). Nanocellulose biopolymer-based biofilms: Applications and challenges. *Biopolymer-Based Nano Films: Applications in Food Packaging and Wound Healing*, 43–62. <https://doi.org/10.1016/B978-0-12-823381-8.00011-9>
- Kabir, E., Kaur, R., Lee, J., Kim, K. H., & Kwon, E. E. (2020). Prospects of biopolymer technology as an alternative option for non-degradable plastics and sustainable management of plastic wastes. *Journal of Cleaner Production*, 258, Article 120536. <https://doi.org/10.1016/J.JCLEPRO.2020.120536>
- Kabir, M. S., Hossain, M. S., Mia, M., Islam, M. N., Rahman, M. M., Hoque, M. B., & Chowdhury, A. M. S. (2018). Mechanical Properties of Gamma-Irradiated Natural Fiber Reinforced Composites. *Nano Hybr. & Compos*, 23, 24–38. <https://doi.org/10.4028/www.scientific.net/nhc.23.24>
- Kalhor, F., Yazdyani, H., Khademorzaeian, F., Hamzkanloo, N., Mokaberi, P., Hosseini, S., & Chamani, J. (2022). Enzyme activity inhibition properties of new cellulose nanocrystals from *Citrus medica* L. pericarp: A perspective of cholesterol lowering. *Luminescence*, 37, 1836–1845. <https://doi.org/10.1002/BIO.4360>
- Kalia, S., Boufi, S., Celli, A., & Kango, S. (2014). Nanofibrillated cellulose: Surface modification and potential applications. *Colloid and Polymer Science*, 292, 5–31. <https://doi.org/10.1007/S00396-013-3112-9> METRICS
- Karak, N. (2012). Vegetable oil-based polymer composites. *Vegetable Oil-Based Polymers*, 247–270. <https://doi.org/10.1533/9780857097149.247>
- Koivuluo, H., Honkanen, M., & Vuoristo, P. (2010). Cold-sprayed copper and tantalum coatings — Detailed FESEM and TEM analysis. *Surface and Coatings Technology*, 204, 2353–2361. <https://doi.org/10.1016/J.SURFOCOAT.2010.01.001>
- Kostic, M., Pejic, B., & Skundric, P. (2008). Quality of chemically modified hemp fibers. *Bioresource Technology*, 99, 94–99. <https://doi.org/10.1016/J.BIOTECH.2006.11.050>
- Kumar, R., Manna, C., Padha, S., Verma, A., Sharma, P., Dhar, A., Ghosh, A., & Bhattacharya, P. (2022). Micro(nano)plastics pollution and human health: How plastics can induce carcinogenesis to humans? *Chemosphere*, 298, Article 134267. <https://doi.org/10.1016/J.CHEMOSPHERE.2022.134267>
- Li, Z., Liu, C.-P., & Yu, T. (2002). Laminate of reformed bamboo and extruded fiber-reinforced cementitious plate. *Journal of Materials in Civil Engineering*, 14, 359–365. [https://doi.org/10.1061/\(ASCE\)0899-1561\(2002\)14:5\(359\)](https://doi.org/10.1061/(ASCE)0899-1561(2002)14:5(359))
- Liu, M., Fernando, D., Daniel, G., Madsen, B., Meyer, A. S., Ale, M. T., & Thygesen, A. (2015). Effect of harvest time and field retting duration on the chemical composition, morphology and mechanical properties of hemp fibers. *Industrial Crops and Products*, 69, 29–39. <https://doi.org/10.1016/J.INDCROP.2015.02.010>
- Lowry, G. V., Hill, R. J., Harper, S., Rawle, A. F., Hendren, C. O., Klaessig, F., Nobmann, U., Sayre, P., & Rumble, J. (2016). Guidance to improve the scientific value of zeta-potential measurements in nanoEHS. *Environmental Science: Nano*, 3, 953–965. <https://doi.org/10.1039/C6EN00136J>
- Lu, N., & Oza, S. (2013). A comparative study of the mechanical properties of hemp fiber with virgin and recycled high density polyethylene matrix. *Composites Part B: Engineering*, 45, 1651–1656. <https://doi.org/10.1016/J.COMPOSITESB.2012.09.076>
- Lu, P., & Hsieh, Y. Lo (2010). Preparation and properties of cellulose nanocrystals: Rods, spheres, and network. *Carbohydrate Polymers*, 82, 329–336. <https://doi.org/10.1016/J.CARBPOL.2010.04.073>
- Maheri, H., Hashemzadeh, F., Shakibapour, N., Kameliya, E., Malaekeh-Nikouei, B., Mokaberi, P., & Chamani, J. (2022). Glucokinase activity enhancement by cellulose nanocrystals isolated from jujube seed: A novel perspective for type II diabetes

- mellitus treatment (In vitro). *Journal of Molecular Structure*, 1269, Article 133803. <https://doi.org/10.1016/J.MOLSTRUC.2022.133803>
- Marques, G., Renocret, J., Gutiérrez, A., & del Río, J. C. (2010). Evaluation of the chemical composition of different non-woody plant fibers used for pulp and paper manufacturing. *The Open Agriculture Journal*, 4, 93–101. <https://doi.org/10.2174/1874331501004010093>
- Mishra, S., Mohanty, A. K., Drzal, L. T., Misra, M., & Hinrichsen, G. (2004). A review on pineapple leaf fibers, sisal fibers and their biocomposites. *Macromolecular Materials and Engineering*, 289, 955–974. <https://doi.org/10.1002/MAME.200400132>
- Mondal, S. (2017). Preparation, properties and applications of nanocellulosic materials. *Carbohydrate Polymers*, 163, 301–316. <https://doi.org/10.1016/J.CARBPOL.2016.12.050>
- Naim, A., Tan, C. S. Y., & Liew, F. K. (2022). Thermal Properties of bamboo cellulose isolated from bamboo culms and shoots. *BioResources*, 17, 4806–4815. <https://doi.org/10.15376/BIORES.17.3.4806-4815>
- Nallusamy, S., & Manoj Babu, A. (2016). X-ray diffraction and FESEM analysis for mixture of hybrid nanoparticles in heat transfer applications. *Journal of Nano Research*, 37, 58–67. <https://doi.org/10.4028/WWW.SCIENTIFIC.NET/JNANOR.37.58>
- Ng, H. M., Sin, L. T., Tee, T. T., Bee, S. T., Hui, D., Low, C. Y., & Rahmat, A. R. (2015b). Extraction of cellulose nanocrystals from plant sources for application as reinforcing agent in polymers. *Composites Part B: Engineering*, 75, 176–200. <https://doi.org/10.1016/J.COMPOSITESB.2015.01.008>
- North, E. J., & Halden, R. U. (2013). Plastics and environmental health: The road ahead. *Reviews on Environmental Health*, 28, 1–8. <https://doi.org/10.1515/REVEH-2012-0030/MACHINEREADABLELITIGATION/RIS>
- Ng, H. M., Sin, L. T., Tee, T. T., Bee, S. T., Hui, D., Low, C. Y., & Rahmat, A. R. (2015a). Extraction of cellulose nanocrystals from plant sources for application as reinforcing agent in polymers. *Composites Part B: Engineering*, 75, 176–200. <https://doi.org/10.1016/J.COMPOSITESB.2015.01.008>
- Patra, J. K., Das, G., Fraceto, L. F., Campos, E. V. R., Rodriguez-Torres, M. D. P., Acosta-Torres, L. S., Diaz-Torres, L. A., Grillo, R., Swamy, M. K., Sharma, S., Habtemariam, S., & Shin, H. S. (2018). Nano based drug delivery systems: Recent developments and future prospects. *Journal of Nanobiotechnology*, 16(1), 1–33. <https://doi.org/10.1186/S12951-018-0392-8>, 201816.
- Pérez, S., & Samain, D. (2010). Structure and engineering of celluloses. *Advances in Carbohydrate Chemistry and Biochemistry*, 64, 25–116. [https://doi.org/10.1016/S0065-2318\(10\)64003-6](https://doi.org/10.1016/S0065-2318(10)64003-6)
- Rahman, M. M., Hossain, M. I., Ghos, B. C., Gafur, M., Gafur, M. A., Alam, M., Alam, M. A., Uddin, M., Uddin, M. J., Yeasmin, M. S., Hasan, M., Chowdhury, T., Chowdhury, T. A., Rana, G., Rana, G. M. M., Karmakar, A., & Barmon, J. (2024d). Fabrication of CNC-AC bionanosorbents from the residual mass of *Magnolia champaca* l. Bark after methanol extraction for wastewater treatment: Continuous column adsorption study. *Environmental Nanotechnology, Monitoring & Management*, 22, Article 101015. <https://doi.org/10.1016/j.enmm.2024.101015>
- Rahman, M. M. (2024). Waste biomass derived chitosan-natural clay based bionanocomposites fabrication and their potential application on wastewater purification by continuous adsorption: A critical review. *South African Journal of Chemical Engineering*, 48, 214–236. <https://doi.org/10.1016/j.sajce.2024.02.006>
- Rahman, M. M., Hosen Pk, M. E., Waliullah, M., Hossain, M. I., Maniruzzaman, M., & Ghos, B. C. (2024e). Production of cellulose nanocrystals from the waste banana (*M. Oranta*) tree rachis fiber as a reinforcement to fabricate useful bionanocomposite. *Carbohydrate Polymer Technologies and Applications*, 8, Article 100607. <https://doi.org/10.1016/j.carpta.2024.100607>
- Rahman, M. M., Hossain, M. I., Hassan, M. M., Ghos, B. C., Rahman, M., Rahman, M. S., Gafur, M., Gafur, M. A., Alam, M. A., & Zuhane, M. K. A. (2024b). Cellulose nanocrystal (CNC) from okra plant (*Abelmoschus esculentus* L.) stalks as a reinforcement in bionanocomposite fabrication: Extraction, processing, and characterization study. *Carbohydrate Polymer Technologies and Applications*, 8, Article 100581. <https://doi.org/10.1016/j.carpta.2024.100581>
- Rahman, M. M., Islam, M. M., & Maniruzzaman, M. (2023b). Preparation and characterization of biocomposite from modified  $\alpha$ -cellulose of *Agave cantala* leaf fiber by graft copolymerization with 2-hydroxy ethyl methacrylate. *Carbohydrate Polymer Technologies and Applications*, 6, Article 100354. <https://doi.org/10.1016/j.carpta.2023.100354>
- Rahman, M. M., & Maniruzzaman, M. (2019). Preparation of shrimp shell chitosan-clay-nanofilter for the purification of drinking water. *International Journal of Food Engineering and Technology*, 2, 1726. <https://doi.org/10.11648/j.ijfet.20180202.12>
- Rahman, M. M., & Maniruzzaman, M. (2021). Extraction of nanocellulose from Banana Rachis (Agro-waste) and preparation of nanocellulose-clay nanofilter for the industrial wastewater purification. *Journal of Bioremediation & Biodegradation*, 12, 485. <https://doi.org/10.4172/2155-6199.1000485>
- Rahman, M. M., & Maniruzzaman, M. (2023). A new route of production of the mesoporous chitosan with well-organized honeycomb surface microstructure from shrimp waste without destroying the original structure of native shells: Extraction, modification and characterization study. *Results in Engineering*, 19, Article 101362. <https://doi.org/10.1016/j.rineng.2023.101362>
- Rahman, M. M., & Maniruzzaman, M. (2024). Environmentally friendly strength bio-composite preparation by grafting of HEMA onto shrimp chitosan without destroying original microstructure to enrich their physicochemical, thermomechanical, and morphological properties. *South African Journal of Chemical Engineering*, 47, 300–311. <https://doi.org/10.1016/j.sajce.2023.12.005>
- Rahman, M. M., Maniruzzaman, M., Gafur, M. A., Al-Ahmary, K. M., Shawabkeh, A., Alsharif, A., Naznin, S., & Al-Otaibi, J. S. (2024f). Fabrication of chitosan coated bentonite clay multifunctional nanosorbents from waste biomass for the effective elimination of hazardous pollutants from waterbodies: A fixed bed biosorption, mechanism, and mathematical model study. *International Journal of Biological Macromolecules*, 282(6), Article 137439. <https://doi.org/10.1016/j.ijbiomac.2024.137439>
- Rahman, M. M., Maniruzzaman, M., Islam, M. R., & Rahman, M. S. (2018a). Synthesis of nano-cellulose from Okra Fibre and FTIR as well as morphological studies on it. *American Journal of Polymer Science and Technology*, 4, 42–52. <https://doi.org/10.11648/J.AJPST.20180402.11>
- Rahman, M. M., Maniruzzaman, M., & Saha, R. K. (2024 g). A green route of antibacterial films production from shrimp (*Penaeus monodon*) shell waste biomass derived chitosan: Physicochemical, thermomechanical, morphological and antimicrobial activity analysis. *South African Journal of Chemical Engineering*. <https://doi.org/10.1016/j.sajce.2024.11.005>
- Rahman, M. M., Maniruzzaman, M., & Yeasmin, M. S. (2023c). A state-of-the-art review focusing on the significant techniques for naturally available fibers as reinforcement in sustainable bio-composites: Extraction, processing, purification, modification, as well as characterization study. *Results in Engineering*, 20, Article 101511. <https://doi.org/10.1016/j.rineng.2023.101511>
- Rahman, M. M., Maniruzzaman, M., Yeasmin, M. S., Gafur, M. A., Shaikh, M. A. A., Alam, M., Uddin, M. J., Hasan, M., Bashera, M. A., Chowdhury, T. A., Mafta, B., Naim, M. R., Rana, G. M. M., Saha, B. K., & Quddus, M. S. (2023d). Adsorptive abatement of Pb<sup>2+</sup> and crystal violet using chitosan-modified coal nanocomposites: A down flow column study. *Groundwater for Sustainable Development*, 23, Article 101028. <https://doi.org/10.1016/j.gsd.2023.101028>
- Rahman, M. M., Maniruzzaman, M., & Zaman, M. N. (2024c). Fabrication and characterization of environmentally friendly biopolymeric nanocomposite films from cellulose nanocrystal of banana *M. Oranta* (Sagar kala) tree rachis fibers and poly lactic acid: A new route. *South African Journal of Chemical Engineering*, , Article 100619. <https://doi.org/10.1016/j.sajce.2024.10.002>
- Rahman, M. M., Rahman, M. S., 2022. Green synthesis of chitosan from shrimp shell and fabrication of chitosan modified clay nanofilter composite for the purification of drinking water. Doi: 10.13140/RG.2.2.27864.67844.
- Rahman, M. M., Shaikh, M. A. A., Yeasmin, M. S., Gafur, M. A., Hossain, M. I., Alam, M. A., Khan, M. S., Paul, T., & Quddus, M. S. (2024a). Simultaneous removal of Ni<sup>2+</sup> and Congo red from wastewater by crystalline nanocellulose - Modified coal bionanocomposites: Continuous adsorption study with mathematical modeling. *Groundwater for Sustainable Development*, 26, Article 101244. <https://doi.org/10.1016/j.gsd.2024.101244>
- Rahman, M. M., Yeasmin, M. S., Uddin, M. J., Hasan, M., Shaikh, M. A. A., Rahman, M. S., & Maniruzzaman, M. (2023a). Simultaneous abatement of Ni<sup>2+</sup> and Cu<sup>2+</sup> effectively from industrial wastewater by a low cost natural clay-chitosan nanocomposite filter: Synthesis, characterization and fixed bed column adsorption study. *Environmental Nanotechnology, Monitoring & Management*, 20, Article 100797. <https://doi.org/10.1016/j.enmm.2023.100797>
- Rahman, O., Rahman, M. M., & Maniruzzaman, M. (2022). Removal of dye and heavy metals from industrial wastewater by activated charcoal-banana rachis cellulose nanocrystal composite filter. *International Journal of Environmental Analytical Chemistry*, 1–19. <https://doi.org/10.1080/03067319.2022.2039647>
- Rahman, M. M., Islam, M. R., Islam, M. R., Naznin, S., 2018b. Extraction and Characterization of Lipid from Pangus Fish (P. Pangasius) Available in Bangladesh by Solvent Extraction Method. *American Journal of Zoology* 1 (2), 28–34. <https://doi.org/10.11648/j.ajz.20180102.11>
- Ravisankar, R., Naseeruthen, A., Rajalakshmi, A., Raja Annamalai, G., & Chandrasekaran, A. (2014). Application of thermogravimetry-differential thermal analysis (TG-DTA) technique to study the ancient potteries from Vellore dist, Tamilnadu, India. *Spectrochimica Acta Part A: Molecular and Biomolecular Spectroscopy*, 129, 201–208. <https://doi.org/10.1016/J.SAA.2014.02.095>
- Rodrigues, M. O., Abrantes, N., Gonçalves, F. J. M., Nogueira, H., Marques, J. C., & Gonçalves, A. M. M. (2019). Impacts of plastic products used in daily life on the environment and human health: What is known? *Environmental Toxicology and Pharmacology*, 72, Article 103239. <https://doi.org/10.1016/J.ETAP.2019.103239>
- Sampath, U. G. T. M., Ching, Y. C., Chuah, C. H., Singh, R., & Lin, P. C. (2017). Preparation and characterization of nanocellulose reinforced semi-interpenetrating polymer network of chitosan hydrogel. *Cellulose*, 24, 2215–2228. <https://doi.org/10.1007/S10570-017-1251-8>
- Sanjay, M. R., Arpitha, G. R., Naik, L. L., Gopalakrishna, K., Yogesh, B., Sanjay, M. R., Arpitha, G. R., Naik, L. L., Gopalakrishna, K., & Yogesh, B. (2016). Applications of natural fibers and its composites: An overview. *Natural Resources*, 7, 108–114. <https://doi.org/10.4236/NR.2016.73011>
- Scimeca, M., Bischetti, S., Lamsira, H. K., Bonfiglio, R., & Bonanno, E. (2018). Energy dispersive X-ray (EDX) microanalysis: A powerful tool in biomedical research and diagnosis. *European Journal of Histochemistry: EJH*, 62, 89–99. <https://doi.org/10.4081/EJH.2018.2841>
- Seabra, A. B., Bernardes, J. S., Fávaro, W. J., Paula, A. J., & Durán, N. (2018). Cellulose nanocrystals as carriers in medicine and their toxicities: A review. *Carbohydrate Polymers*, 181, 514–527. <https://doi.org/10.1016/J.CARBPOL.2017.12.014>
- Seddiqi, H., Oliaei, E., Honarkar, H., Jin, J., Gezon, L. C., Bacabac, R. G., & Klein-Nulend, J. (2021). Cellulose and its derivatives: Towards biomedical applications. *Cellulose*, 28(4), 1893–1931. <https://doi.org/10.1007/S10570-020-03674-W>, 202128.
- Sharma, M. (2019). Transdermal and intravenous nano drug delivery systems: Present and future. *Applications of Targeted Nano Drugs and Delivery Systems: Nanoscience and Nanotechnology in Drug Delivery*, 499–550. <https://doi.org/10.1016/B978-0-12-814029-1.00018-1>
- Sheikh, M. S., Rahman, M. M., Rahman, M. S., Yildirim, K., & Maniruzzaman, M. (2023). Fabrication of Nano Composite Membrane Filter from Graphene Oxide(GO) and Banana Rachis Cellulose Nano Crystal(CNC) for Industrial Effluent Treatment.

- Journal of Industrial and Engineering Chemistry*, 128, 196–208. <https://doi.org/10.1016/j.jiec.2023.07.048>
- Siró, I., & Plackett, D. (2010). Microfibrillated cellulose and new nanocomposite materials: A review. *Cellulose (London, England)*, 17(3), 459–494. <https://doi.org/10.1007/S10570-010-9405-Y>, 201017.
- Song, J. H., Murphy, R. J., Narayan, R., & Davies, G. B. H. (2009). Biodegradable and compostable alternatives to conventional plastics. *Philosophical Transactions of the Royal Society B: Biological Sciences*, 364, 2127–2139. <https://doi.org/10.1098/RSTB.2008.0289>
- Sreekumar, P. A., Saiah, R., Saiter, J. M., Leblanc, N., Joseph, K., Unnikrishnan, G., & Thomas, S. (2009). Dynamic mechanical properties of sisal fiber reinforced polyester composites fabricated by resin transfer molding. *Polymer Composites*, 30, 768–775. <https://doi.org/10.1002/PC.20611>
- Stelte, W., & Sanadi, A. R. (2009). Preparation and characterization of cellulose nanofibers from two commercial hardwood and softwood pulps. *Industrial and Engineering Chemistry Research*, 48, 11211–11219. <https://doi.org/10.1021/IE9011672>
- Tavana, S., Riyahi, A., Nikjoo, S., Shafi-Moghaddam, S., Taheri, R., Akhavannezhad, Z., Mokaberi, P., & Chamani, J. (2024). Synthesis and characterization of cellulose nanocrystals derived from ginger stick for berberine delivery: Exploring interactions with human holo-transferrin. *Colloid and Polymer Science*, 302, 1617–1633. <https://doi.org/10.1007/S00396-024-05297-0/METRICS>
- Tengsuthiwat, J., Raghunathan, V., Ayyappan, V., Techawinyutham, L., Srisuk, R., Yorseng, K., Rangappa, S. M., & Siengchin, S. (2024a). Lignocellulose sustainable composites from agro-waste Asparagus bean stem fiber for polymer casting applications: Effect of fiber treatment. *International Journal of Biological Macromolecules*, 278, Article 134884. <https://doi.org/10.1016/j.ijbiomac.2024.134884>
- Tengsuthiwat, J., Vinod, A., Vijay, R., Yashas Gowda, T. G., Rangappa, S. M., & Siengchin, S. (2024b). Characterization of novel natural cellulose fiber from Ficus macrocarpa bark for lightweight structural composite application and its effect on chemical treatment. *Helijon*, 10, e30442. <https://doi.org/10.1016/j.helijon.2024.e30442>
- Thakur, M., Sharma, A., Ahlawat, V., Bhattacharya, M., & Goswami, S. (2020). Process optimization for the production of cellulose nanocrystals from rice straw derived  $\alpha$ -cellulose. *Materials Science for Energy Technologies*, 3, 328–334. <https://doi.org/10.1016/J.MSET.2019.12.005>
- Trache, D., Hussin, M. H., Haafiz, M. K. M., & Thakur, V. K. (2017). Recent progress in cellulose nanocrystals: Sources and production. *Nanoscale*, 9, 1763–1786. <https://doi.org/10.1039/C6NR09494E>
- Vinod, A., Sanjay, M. R., & Siengchin, S. (2023). Recently explored natural cellulosic plant fibers 2018–2022: A potential raw material resource for lightweight composites. *Industrial Crops and Products*, 192, Article 116099. <https://doi.org/10.1016/j.indcrop.2022.116099>
- Vinod, A., Sanjay, M. R., Suchart, S., & Jyotishkumar, P. (2020). Renewable and sustainable biobased materials: An assessment on biofibers, biofilms, biopolymers and biocomposites. *Journal of Cleaner Production*, 258, Article 120978. <https://doi.org/10.1016/j.jclepro.2020.120978>
- Whittig, L. D., & Allardice, W. R. (2018). X-Ray Diffraction Techniques. *Methods of Soil Analysis, Part 1: Physical and Mineralogical Methods*, 331–362. <https://doi.org/10.2136/SSSABOOKSER5.1.2ED.C12>
- Williams, H. (2021). SEM for conductive and non-conductive specimens. *Physics Education*, 56, Article 055034. <https://doi.org/10.1088/1361-6552/AC1503>
- Xu, R. (2008). Progress in nanoparticles characterization: Sizing and zeta potential measurement. *Particuology*, 6, 112–115. <https://doi.org/10.1016/J.PARTIC.2007.12.002>
- Zhao, G., Du, J., Chen, W., Pan, M., & Chen, D. (2019). Preparation and thermostability of cellulose nanocrystals and nanofibrils from two sources of biomass: Rice straw and poplar wood. *Cellulose*, 26, 8625–8643. <https://doi.org/10.1007/S10570-019-02683-8/METRICS>